

# High-Order Schemes for Hyperbolic Conservation Laws Using Young Measures

Shaoshuai Chu\* and Michael Herty†

## Abstract

We develop high-order numerical schemes to solve random hyperbolic conservation laws using linear programming. The proposed schemes are high-order extensions of the existing first-order scheme introduced in [S. CHU, M. HERTY, M. LUKÁČOVÁ-MEDVID'OVÁ, AND Y. ZHOU, solving random hyperbolic conservation laws using linear programming], where a novel structure-preserving numerical method using a concept of generalized, measure-valued solutions to solve random hyperbolic systems of conservation laws is proposed, yielding a linear partial differential equation concerning the Young measure and allowing the computation of approximations based on linear programming problems. The second-order extension is obtained using piecewise linear reconstructions of the one-sided point values of the unknowns. The fifth-order scheme is developed using the finite-difference alternative weighted essentially non-oscillatory (A-WENO) framework. These extensions significantly improve the resolution of discontinuities, as demonstrated by a series of numerical experiments on both random (Burgers equation, isentropic Euler equations) and deterministic (discontinuous flux, pressureless gas dynamics, Burgers equation with non-atomic support) hyperbolic conservation laws.

**Key words:** Nonlinear hyperbolic systems with uncertainty, random parameterized Young measures, linear programming problems, piecewise linear reconstructions, A-WENO schemes

**AMS subject classification:** 60C50, 60H35, 82C40, 35L65, 65M06, 65M08

## 1 Introduction

This paper focuses on numerical solutions of random hyperbolic conservation laws, which arise in various fields including engineering, atmospheric, and geophysical applications. It is well known that these systems often develop complex wave patterns, including discontinuities such as shocks and rarefaction waves, even when the initial data are very smooth, which introduces significant challenges in designing suitable numerical methods to solve systems.

In the last two decades, a series of numerical methods have been proposed for solving random conservation laws, including the non-intrusive (Quasi-) Monte Carlo simulations, stochastic collocation, and (intrusive) generalized polynomial chaos expansion; see, e.g., [1, 3, 31, 42, 46, 47, 49, 51, 60–62] and the references therein. Monte Carlo methods are widely valued for their robustness, though they are not always computationally efficient. The stochastic collocation method benefits from straightforward applicability, as it allows existing deterministic numerical solvers to be reused with minimal adaptation. In contrast, intrusive approaches such as stochastic Galerkin methods, which rely on generalized polynomial chaos expansions (gPC), impose greater constraints. These methods require projecting the governing equations onto a gPC basis, generating an expanded deterministic system for the expansion coefficients [50, 59]. Although this intrusive approach can achieve high accuracy with low polynomial degrees for smooth solutions [23, 24], it faces two key challenges. First, the resulting coupled system for

\*Department of Mathematics, RWTH Aachen University, 52056, Aachen, Germany; chu@igpm.rwth-aachen.de

†Department of Mathematics, RWTH Aachen University, 52056, Aachen, Germany; Department of Mathematics and Applied Mathematics, University of Pretoria, Private Bag X20, Hatfield 0028, South Africa; herty@igpm.rwth-aachen.de

gPC coefficients may lose hyperbolicity, complicating its numerical solution [9, 20, 21, 31, 32, 35]. Second, the method demands significant re-implementation of the deterministic solver, as the governing equations must be reformulated and projected onto the gPC basis, creating substantial implementation overhead. At the same time, both stochastic collocation and Galerkin methods are susceptible to Gibbs phenomena near discontinuities due to their spectral approximation frameworks. Mitigating these oscillations often requires additional techniques such as spectral filtering [5, 20, 36, 42, 54], spectral viscosity [30, 58], or adaptive diffusion [10, 15, 39]. The advantages and disadvantages of different approaches have been extensively discussed in the literature, and we refer to [10] for recent discussions.

In [12], a novel numerical approach based on a measure-valued framework is proposed using parameterized Young measures (YM) rather than traditional weak (distributional) solutions [25, 26] (see also [22], where the concept of measure-valued solutions for conservation laws was introduced in a rigorous analytical framework and has inspired numerous developments). This reformulation transforms the problem into a linear optimization problem, circumventing several challenges associated with existing methods. Inspired by recent advances in dissipative measure-valued solutions for compressible fluid flows, the approach directly computes the YM within the numerical scheme, unlike previous methods where it emerges from weakly convergent approximations. Additionally, while previous works (see, e.g., [7]) approximate YM moments using multiple entropy functions—often unavailable for general hyperbolic systems—this method considers only moments in the random dimension, enabling standard finite-volume schemes for moment propagation. Compared to existing moment-based approaches to random conservation laws, see; e.g., [41, 42], it introduces a different closure formulation that eliminates the need for filters and extends naturally to systems of equations. The proposed method has been applied so far only to one-dimensional (1-D) hyperbolic conservation laws, including the isentropic Euler system and Burgers equation. In this paper, we extend the discussion to a series of further problems as well as high-order finite-volume (FV) and finite-difference (FD) methods.

The approach introduced in [12], uses a FV Lax-Friedrichs fluxes, offers a robust and accurate tool for solving random nonlinear conservation laws. However, it is only first-order accurate and requires very fine meshes to achieve the desired resolution for shock waves and other complex wave structures. In order to address this issue, in this paper, we adopt the semi-discretization form and extend the first-order approach to higher orders (second and fifth) of accuracy by employing high-order local Lax-Friedrichs (LLF) fluxes in the spatial dimension. The second-order extension is achieved through applying piecewise linear reconstruction to reconstruct the one-sided point values of the unknowns, and a fifth-order scheme is developed within the FD essentially non-oscillatory (A-WENO) framework. The latter has been proven to be a powerful tool for generalizing low-order FV schemes to higher-order FD ones; see, e.g., [18, 37, 38, 44]. In order to reduce non-physical oscillations, we use the local characteristic decomposition (LCD) in the high-order interpolation as done in [8, 14, 38, 44, 52, 56]. For evolving the numerical solution in time, we solve the system of ordinary differential equations (ODEs) using a standard three-stage third-order strong stability preserving Runge-Kutta (SSP RK3) solver; see, e.g., [33, 34].

The studied higher-order schemes are applied to a series of numerical examples, including both random and deterministic hyperbolic conservation laws. In the random case, the obtained results of Burgers equation and isentropic Euler equations of gas dynamics clearly demonstrate the robustness and higher efficiency of the studied high-order schemes. The schemes have also been tested on several challenging examples including discontinuous flux, pressureless gas dynamics, and Burgers equation with non-atomic support. Conservation laws with discontinuous flux arise in numerous applications, including multi-phase flows in heterogeneous porous media and traffic flows on highways with varying surface conditions. The mathematical and numerical analysis of such problems is highly challenging, as many difficulties already appear in the simplest case of 1-D scalar conservation laws with discontinuous flux. As demonstrated in [2, 45], systems of conservation laws with discontinuous flux may admit multiple entropy solutions and exhibit small-scale dependent shock waves. The pressureless gas dynamics system is only weakly hyperbolic, and its solutions develop delta-shocks and vacuum states in finite time, which makes the design of stable and accurate numerical methods particularly challenging; see, e.g. [4, 55]. Finally, the solutions of the Burgers equation are genuinely measure-

valued and cannot be represented by atomic states. Standard numerical methods tend to collapse such distributions into atomic solutions, making it challenging to design schemes that accurately capture the non-atomic structure; see, e.g., [22, 27, 28]. The obtained numerical results demonstrate that the designed schemes can be applied to these examples and the resolution of the computed solution improves significantly when higher-order schemes are used.

The paper is organized as follows. In §2, we briefly review the existing first-order Lax-Friedrichs YM scheme. In §3, we extend the first-order scheme to second order. In §4, we show the fifth-order extension in the framework of A-WENO scheme. Finally, in §5, we apply the designed schemes to a number of numerical examples to demonstrate the performance of the studied schemes for both random and deterministic hyperbolic conservation laws.

## 2 First-Order Lax–Friedrichs Scheme: A Brief Overview

In this section, we briefly describe the existing first-order Lax–Friedrichs scheme from [12] for solving the random hyperbolic conservation laws, which in the 1-D case, read as

$$\mathbf{u}_t + \mathbf{f}(\mathbf{u})_x = 0, \quad (2.1)$$

with the initial conditions

$$\mathbf{u}(x, \xi, 0) = \psi(x, \xi),$$

where  $t$  is the time,  $x$  is the spatial variable,  $\xi \in \Omega$  is the randomness parameter,  $\mathbf{u} = (u^{(1)}, \dots, u^{(n)})^\top$  is a vector of unknowns and  $\mathbf{f} : \mathbb{R}^n \rightarrow \mathbb{R}^n$  is the non-linear flux. The system (2.1) is assumed to be hyperbolic; see, e.g., [6, 19]. We also assume that (2.1) is accompanied by a convex entropy  $\eta$  and the corresponding entropy flux pair  $q$  satisfying the entropy inequality

$$\partial_t \eta(\mathbf{u}(x, \xi, t)) + \partial_x q(\mathbf{u}(x, \xi, t)) \leq 0.$$

Assume that  $\xi \sim \mathcal{U}(\Omega)$ , that is,  $\xi$  is uniformly distributed and  $p(\xi) = p_0 \equiv \frac{1}{|\Omega|}$ , and  $\{\xi_i\}_{i=1}^{N_\xi}$  are equidistant points in  $\Omega$ . To illustrate the strategy for a fully discrete approximation, we consider piecewise constant orthonormal basis functions  $\phi_i$  mimicking the stochastic collocation approach,

$$\phi_i(\xi) = \frac{1}{p_0 \Delta \xi} \chi_{[\xi_i - \frac{\Delta \xi}{2}, \xi_i + \frac{\Delta \xi}{2}]}(\xi), \quad i = 1, \dots, N_\xi.$$

Furthermore, we consider a discretization with  $N_u$  equidistant points  $\mathbf{u}_\ell \in \mathbb{R}^n$  of the solution space for  $\mathbf{u}(x, \xi, t) \in \mathbb{R}^n$ .

For given moments  $\mathbf{u}_{i,j}^n$ , a discrete approximation  $\mu_{i,\ell}^*$  to the measure-valued solution  $\mu_\xi^*(\mathbf{u}_\ell; \mathbf{u}_j^n)$  of the linear programming problem needs to be computed with  $\mathbf{u}_j^n = (\mathbf{u}_{1,j}^n, \dots, \mathbf{u}_{N_\xi,j}^n)^\top$ . The values of  $\mu_{i,\ell}^*$  are approximated by solving the following linear programming problem reading for the unknowns  $\{\mu_{i,\ell}\}_{i=1, \dots, N_\xi, \ell=1, \dots, N_u}$ :

$$\{\mu_{i,\ell}^*(\mathbf{u}_j^n)\} = \operatorname{argmin}_{\{\mu_{i,\ell}\}} \Delta \xi \Delta \mathbf{u} \sum_{i=1}^{N_\xi} \sum_{\ell=1}^{N_u} \eta(\mathbf{u}_\ell) p_0 \mu_{i,\ell} \quad (2.2a)$$

$$\text{subject to } \mu_{i,\ell} \geq 0, \forall (i, \ell), \quad (2.2b)$$

$$\mu_{i,\ell} \leq \lambda_F / \Delta \mathbf{u}, \forall (i, \ell), \quad (2.2c)$$

$$\Delta \mathbf{u} \sum_{\ell=1}^{N_u} \mu_{i,\ell} = 1, \forall i, \quad (2.2d)$$

$$\Delta \mathbf{u} \sum_{\ell=1}^{N_u} \mathbf{u}_\ell \mu_{i,\ell} = \mathbf{u}_{i,j}^n, \forall i, \quad (2.2e)$$

where  $\Delta \mathbf{u}$  is the discretization in phase space of  $\mathbf{u}$ . We note that the upper bound on  $\mu_{i,\ell}$  (2.2c) is in fact obtained by the non-negativity (2.2b) and (2.2d). For solving the linear programming problem, we use the black-box solver `linprog` of Matlab R2023b.

**Remark 2.1** Here,  $0 < \lambda_F \leq 1$  is a factor controlling the support of the YM and the case  $\lambda_F = 1$  corresponds to the case where atomic solutions are allowed.

**Remark 2.2** Notice that the accuracy of the approximated values of  $\mu_{i,\ell}^*$  depends on the tolerance error of the black-box solver `linprog`, in all of the examples reported in §5, we use the default settings of this function.

We then update the moments  $\mathbf{u}_{i,j}^{n+1}$  at the next time level using the first-order Lax-Friedrichs FV method:

$$\mathbf{u}_{i,j}^{n+1} = \frac{1}{2}(\mathbf{u}_{i,j+1}^n + \mathbf{u}_{i,j-1}^n) - \frac{\Delta t}{2\Delta x} (\mathbf{F}_{i,j+1}^n - \mathbf{F}_{i,j-1}^n).$$

Here,  $\mathbf{F}_{i,j}^n$  are the numerical fluxes given by

$$\mathbf{F}_{i,j}^n = \Delta \mathbf{u} \sum_{\ell=1}^{N_u} \mathbf{f}(\mathbf{u}_\ell) \mu_{i,\ell}^*(\mathbf{u}_j^n), \quad (2.3)$$

and  $\Delta t$  is determined by the CFL condition

$$\max_{i=1,\dots,N_\xi, j=1,\dots,N_x} \left\{ \Delta \xi \sum_{i=1}^{N_x} \Delta \mathbf{u} \sum_{\ell=1}^{N_u} \sigma_{ij} \mu_{i,\ell}^*(\mathbf{u}_j^n) p_0 \right\} \Delta t = \text{CFL} \Delta x,$$

where  $\sigma = \max\{|\lambda_1(A)| \dots |\lambda_n(A)|\}$ , and  $\lambda_k(A)$  for  $k = 1, \dots, n$  are the eigenvalues of the Jacobian  $A = \frac{\partial \mathbf{f}}{\partial \mathbf{u}}$ . We refer the readers to [12] for more details on the introduction of the approach.

### 3 Second-Order Local Lax–Friedrichs (LLF) Scheme

We now extend the first-order Lax-Friedrichs scheme introduced in §2 to the second-order of accuracy. The moments  $\mathbf{u}_{i,j}^n$  (in the rest of the paper, we will suppress the time-dependence of all of the indexed quantities for the sake of brevity) of the 1-D random hyperbolic conservation laws (2.1) are evolved in time by solving the following system of ordinary partial differential equations (ODEs)

$$\frac{d\mathbf{u}_{i,j}}{dt} = -\frac{\mathcal{F}_{i,j+\frac{1}{2}} - \mathcal{F}_{i,j-\frac{1}{2}}}{\Delta x}. \quad (3.1)$$

Here,  $\mathcal{F}_{i,j+\frac{1}{2}} = \mathcal{F}_{i,j+\frac{1}{2}}(\mathbf{u}_{i,j+\frac{1}{2}}^{-,*}, \mathbf{u}_{i,j+\frac{1}{2}}^{+,*})$  stand for the FV LLF fluxes (see [40, 53]):

$$\mathcal{F}_{i,j+\frac{1}{2}} = \frac{\mathbf{f}(\mathbf{u}_{i,j+\frac{1}{2}}^{-,*}) + \mathbf{f}(\mathbf{u}_{i,j+\frac{1}{2}}^{+,*})}{2} - \frac{a_{i,j+\frac{1}{2}}}{2} (\mathbf{u}_{i,j+\frac{1}{2}}^{+,*} - \mathbf{u}_{i,j+\frac{1}{2}}^{-,*}), \quad (3.2)$$

where  $\mathbf{u}_{i,j+\frac{1}{2}}^{\pm,*}$  are the one-sided point values of  $\mathbf{u}_{i,j}^* = \Delta \mathbf{u} \sum_{\ell=1}^{N_u} \mathbf{u}_\ell \mu_{i,\ell}^*(\mathbf{u}_j^n)$  at the cell interface  $(\xi, x) = (\xi_i, x_{j+\frac{1}{2}})$  estimated using a piecewise linear interpolant:

$$\tilde{\mathbf{u}}^*(x) = \mathbf{u}_{i,j}^* + (\mathbf{u}_x^*)_{i,j}(x - x_j), \quad (3.3)$$

which leads to

$$\mathbf{u}_{i,j+\frac{1}{2}}^{-,*} = \mathbf{u}_{i,j}^* + \frac{\Delta x}{2} (\mathbf{u}_x^*)_{i,j}, \quad \mathbf{u}_{i,j-\frac{1}{2}}^{+,*} = \mathbf{u}_{i,j}^* - \frac{\Delta x}{2} (\mathbf{u}_x^*)_{i,j}. \quad (3.4)$$

Here, the values of  $\mu_{i,\ell}^*(\mathbf{u}_j^n)$  are obtained by solving the linear programming (2.2a)–(2.2e).

In order to ensure the non-oscillatory nature of the reconstruction (3.4)–(3.5), the slopes  $(\mathbf{u}_x^*)_{i,j}$  in (3.3) need to be computed with the help of a nonlinear limiter. In all of the numerical experiments reported in §5, we have used a generalized minmod limiter [43, 48, 57]:

$$(\mathbf{u}_x^*)_{i,j} = \text{minmod} \left( \theta \frac{\mathbf{u}_{i,j}^* - \mathbf{u}_{i,j-1}^*}{\Delta x}, \frac{\mathbf{u}_{i,j+1}^* - \mathbf{u}_{i,j-1}^*}{2\Delta x}, \theta \frac{\mathbf{u}_{i,j+1}^* - \mathbf{u}_{i,j}^*}{\Delta x} \right), \quad \theta \in [1, 2], \quad (3.5)$$

applied in a component-wise manner. Here, the minmod function is defined as

$$\text{minmod}(z_1, z_2, \dots) := \begin{cases} \min_j \{z_j\} & \text{if } z_j > 0 \quad \forall j, \\ \max_j \{z_j\} & \text{if } z_j < 0 \quad \forall j, \\ 0 & \text{otherwise.} \end{cases} \quad (3.6)$$

The parameter  $\theta$  in (3.6) is used to control the amount of numerical viscosity present in the resulting scheme. In general, larger values of  $\theta$  correspond to sharper but, in general, more oscillatory reconstructions. In all of the numerical examples reported in §5, we take  $\theta = 1.5$ .

Finally, the local speed of propagation  $a_{i,j+\frac{1}{2}}$  is estimated using the eigenvalues  $\lambda_1(A) \leq \dots \leq \lambda_d(A)$  of the Jacobian  $A = \frac{\partial \mathbf{f}}{\partial \mathbf{u}}$ , defined by

$$a_{i,j+\frac{1}{2}} = \max_j \left\{ |\lambda_1(\mathbf{u}_{i,j+\frac{1}{2}}^{-,*})|, |\lambda_1(\mathbf{u}_{i,j+\frac{1}{2}}^{+,*})|, |\lambda_d(\mathbf{u}_{i,j+\frac{1}{2}}^{-,*})|, |\lambda_d(\mathbf{u}_{i,j+\frac{1}{2}}^{+,*})| \right\}.$$

**Remark 3.1** *The LLF fluxes given by (3.2) can also be replaced by*

$$\mathcal{F}_{i,j+\frac{1}{2}} = \frac{\Delta \mathbf{u} \sum_{\ell=1}^{N_u} \mathbf{f}(\mathbf{u}_\ell)(\mu_{i,\ell}^*)^- + \Delta \mathbf{u} \sum_{\ell=1}^{N_u} \mathbf{f}(\mathbf{u}_\ell)(\mu_{i,\ell}^*)^+}{2} - \frac{a_{i,j+\frac{1}{2}}}{2} (\mathbf{u}_{i,j+\frac{1}{2}}^{+,*} - \mathbf{u}_{i,j+\frac{1}{2}}^{-,*}), \quad (3.7)$$

where

$$\mathbf{u}_{i,j+\frac{1}{2}}^{-,*} = \Delta \mathbf{u} \sum_{\ell=1}^{N_u} (\mathbf{u}_\ell)(\mu_{i,\ell}^*)^-, \quad \text{and} \quad \mathbf{u}_{i,j+\frac{1}{2}}^{+,*} = \Delta \mathbf{u} \sum_{\ell=1}^{N_u} (\mathbf{u}_\ell)(\mu_{i,\ell}^*)^+, \quad (3.8)$$

and  $(\mu_{i,\ell}^*)^-$  and  $(\mu_{i,\ell}^*)^+$  are obtained by solving the linear programming (2.2a)–(2.2e) but with  $\mathbf{u}_{i,j}$  in (2.2e) replaced by  $\mathbf{u}_{i,j+\frac{1}{2}}^-$  and  $\mathbf{u}_{i,j+\frac{1}{2}}^+$ , respectively. The values of  $\mathbf{u}_{i,j+\frac{1}{2}}^\pm$  are the one-sided point values of  $\mathbf{u}_{i,j}$  at the cell interface  $(\xi, x) = (\xi_i, x_{j+\frac{1}{2}})$  estimated using the piecewise linear interpolant (3.3)–(3.6).

It is noted that the numerical results computed by the LLF fluxes (3.2) and (3.7) coincide, which will be demonstrated in one example in §5. However, one can clearly see that the computations of LLF fluxes (3.2) are computationally much cheaper than (3.7) since it only needs to solve the linear programming problem once, which can save around half of the CPU times.

**Remark 3.2** Notice that applying the minmod limiter to the piecewise linear interpolation (3.3)–(3.6) with large values of  $\theta$  directly may lead to relatively large oscillations in the computed solution. In order to suppress these spurious oscillations, we apply the minmod limiter to the local characteristic variables, which are obtained using the LCD based linear interpolation (see, e.g., [11, 16, 38, 52, 56] and references therein); see Appendix A for details.

## 4 Fifth-Order Local Lax–Friedrichs (LLF) Scheme

In this section, we extend the second-order scheme introduced in §3 to the fifth order of accuracy in the framework of the FD A-WENO scheme introduced in [38] (see also [44]), which has been proven to be a powerful tool for generalizing low-order FV schemes to higher-order FD ones.

According to [38], the point values  $\mathbf{u}_{i,j}$  are evolved in time by solving the following system of ODEs:

$$\frac{d\mathbf{u}_{i,j}}{dt} = -\frac{\mathcal{H}_{i,j+\frac{1}{2}} - \mathcal{H}_{i,j-\frac{1}{2}}}{\Delta x}, \quad (4.1)$$

where  $\mathcal{H}_{i,j+\frac{1}{2}}$  is the (fifth-order accurate) numerical flux defined by

$$\mathcal{H}_{i,j+\frac{1}{2}} = \mathcal{F}_{i,j+\frac{1}{2}} - \frac{1}{24}(\Delta x)^2 (\mathbf{F}_{xx})_{i,j+\frac{1}{2}} + \frac{7}{5760}(\Delta x)^4 (\mathbf{F}_{xxxx})_{i,j+\frac{1}{2}}. \quad (4.2)$$

Here,  $\mathcal{F}_{i,j+\frac{1}{2}}$  is the FV numerical flux as in (3.2),  $(\mathbf{F}_{xx})_{i,j+\frac{1}{2}}$  and  $(\mathbf{F}_{xxxx})_{i,j+\frac{1}{2}}$  are the higher-order correction term computed by the fourth- and second-order accurate FDs, respectively; see, e.g., [13, 17, 18, 29]. In this paper, we have used the following new more efficient higher-order correction terms from [18]:

$$\begin{aligned} (\mathbf{F}_{xx})_{i,j+\frac{1}{2}} &= \frac{1}{12(\Delta x)^2} \left[ -\mathcal{F}_{i,j-\frac{3}{2}} + 16\mathcal{F}_{i,j-\frac{1}{2}} - 30\mathcal{F}_{i,j+\frac{1}{2}} + 16\mathcal{F}_{i,j+\frac{3}{2}} - \mathcal{F}_{i,j+\frac{5}{2}} \right], \\ (\mathbf{F}_{xxxx})_{i,j+\frac{1}{2}} &= \frac{1}{(\Delta x)^4} \left[ \mathcal{F}_{i,j-\frac{3}{2}} - 4\mathcal{F}_{i,j-\frac{1}{2}} + 6\mathcal{F}_{i,j+\frac{1}{2}} - 4\mathcal{F}_{i,j+\frac{3}{2}} + \mathcal{F}_{i,j+\frac{5}{2}} \right], \end{aligned} \quad (4.3)$$

which are computed using the FV numerical fluxes  $\mathcal{F}_{i,j+\frac{1}{2}}$ , and have been proved to be more efficient than the old version (see (4.4) below), while affect neither the accuracy nor the quality of resolution.

**Remark 4.1** As in the second-order scheme in §3, one can also use the FV numerical fluxes  $\mathcal{F}_{i,j+\frac{1}{2}}$  defined by (3.7)–(3.8), but it is more computationally expensive. At the same time, to ensure that the obtained numerical scheme (4.1)–(4.3) is of the fifth order of accuracy, the one-sided point values  $\mathbf{u}_{i,j+\frac{1}{2}}^{-,*}$  and  $\mathbf{u}_{i,j+\frac{1}{2}}^{+,*}$ , or  $\mathbf{u}_{i,j+\frac{1}{2}}^-$  and  $\mathbf{u}_{i,j+\frac{1}{2}}^+$ , employed to compute the numerical flux  $\mathcal{F}_{i,j+\frac{1}{2}}$  need to be at least fifth order accurate. This can be done by using a certain nonlinear limiting procedure like the fifth-order WENO-Z interpolation from [29, 38, 44] applied to the local characteristic variables; see Appendix B for details.

**Remark 4.2** The high-order correction terms  $(\mathbf{F}_{xx})_{i,j+\frac{1}{2}}$  and  $(\mathbf{F}_{xxxx})_{i,j+\frac{1}{2}}$  in (4.2) can also be computed by

$$\begin{aligned} (\mathbf{F}_{xx})_{i,j+\frac{1}{2}} &= \frac{1}{48(\Delta x)^2} (-5\mathbf{F}_{i,j-2} + 39\mathbf{F}_{i,j-1} - 34\mathbf{F}_{i,j} - 34\mathbf{F}_{i,j+1} + 39\mathbf{F}_{i,j+2} - 5\mathbf{F}_{i,j+3}) \\ (\mathbf{F}_{xxxx})_{i,j+\frac{1}{2}} &= \frac{1}{2(\Delta x)^4} (\mathbf{F}_{i,j-2} - 3\mathbf{F}_{i,j-1} + 2\mathbf{F}_{i,j} + 2\mathbf{F}_{i,j+1} - 3\mathbf{F}_{i,j+2} + \mathbf{F}_{i,j+3}), \end{aligned} \quad (4.4)$$

where  $\mathbf{F}_{i,j}$  are defined by (2.3).

Notice that the main difference between (4.3) and (4.4) is that in (4.3), we compute the high-order correction terms  $(\mathbf{F}_{xx})_{i,j+\frac{1}{2}}$  and  $(\mathbf{F}_{xxxx})_{i,j+\frac{1}{2}}$  terms with the help of the FV numerical fluxes  $\mathcal{F}_{i,j+\frac{1}{2}}$  instead of the point values  $\mathbf{F}_{i,j}$ . One can clearly see that (4.3) is computationally much cheaper than (4.4) as there is no need to compute the point values  $\mathbf{F}_{i,j}$ , where the term  $\mu_{i,\ell}^*(\mathbf{u}_j^n)$  is obtained by solving the linear programming problem (2.2a)–(2.2e).

**Remark 4.3** In this paper, we extend the second order scheme to the fifth order of accuracy in the framework of FD A-WENO methods, but it is also easy to extend it to even higher-order accuracy in this framework.

## 5 Numerical Examples

In this section, we apply the studied first-, second-, and fifth-order schemes to several numerical examples to demonstrate the superiority and robustness of the studied high-order schemes. For the sake of brevity, the tested first-, second-, and fifth-order schemes will be referred to as the 1-, 2-, and 5-Order schemes, respectively. As in [12], we present the results obtained using both the YM and stochastic collocation (which will be referred to as collocation) methods, as a comparison. We numerically integrate semi-discrete ODE systems (3.1) and (4.1) using the SSP RK3 method and use the CFL number 0.45 in all examples. We take  $\lambda_F = 1$  in Examples 1–6 and 0.05 in Example 7.

### 5.1 Numerical Examples for Random Hyperbolic Conservation Laws

We first apply the studied YM and collocation schemes to a number of numerical examples for random hyperbolic conservation laws, including the Burgers equation and isentropic Euler system to show the validity of the YM formulation.

### 5.1.1 Burgers Equation

In this section, we consider the 1-D Burgers equation

$$u_t + \left( \frac{u^2}{2} \right)_x = 0. \quad (5.1)$$

The corresponding entropy function  $\eta$  in (2.2a) is defined by  $\eta = \frac{1}{2}u^2$ .

**Example 1.** In the first example taken from [12], we consider the Burgers equation (5.1) with the following initial data

$$u(x, \xi, 0) = \xi \sin(2\pi x),$$

prescribed in the computational domain  $[0, 1] \times [-1, 1]$  subject to the free boundary conditions. We plot the initial data in Figure 5.1 and note that even though the initial data are smooth, a shock will be formed at later time  $t > 0$  for any  $\xi > 0$ . For  $\xi < 0$ , the solution remains smooth.

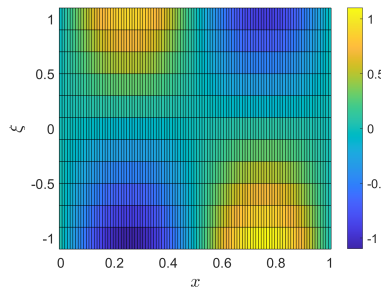


Figure 5.1: Example 1: Initial data.

We compute the numerical solutions until the final time  $t = 0.25$  by the studied 1-, 2-, and 5-Order YM schemes on the uniform mesh with  $N_x = 100$  and  $N_\xi = 10$ . For the discretization in phase space, we set  $u \in [-1.5, 1.5]$  and  $N_u = 100$ . The numerical results obtained are presented in Figure 5.2 together with the numerical results computed by the corresponding location approaches, where we present the results from a top-view perspective to enhance visualization of the resolution near the shock wave. One can clearly see that the resolution of the computed results near the shock waves improves significantly with the use of high-order schemes, especially when transiting from the 1-Order scheme to the 2-Order one.

### 5.1.2 Isentropic Euler System

In this section, we consider the 1-D isentropic Euler system, which reads as

$$\begin{cases} \rho_t + q_x = 0, \\ q_t + \left( \frac{q^2}{\rho} + p \right)_x = 0, \end{cases} \quad (5.2)$$

where  $\rho$ ,  $v := \frac{q}{\rho}$ , and  $p$  are the density, velocity, and pressure, respectively. The system is completed through the following equation of state:

$$p = \kappa \rho^\gamma, \quad (5.3)$$

where  $\kappa$  is a constant, and  $\gamma$  represents the specific heat ratio. In all of the numerical experiments reported in this section, we have used  $\kappa = 1$  and  $\gamma = 1.5$ . The corresponding entropy function  $\eta$  in (2.2a) is defined by  $\eta = \frac{1}{2}\rho v^2 + \frac{p}{\gamma-1}$ .

**Remark 5.1** As mentioned in §3 and §4, we use the LCD based piecewise linear interpolation in the 2-Order scheme and WENO-Z interpolation in the 5-Order scheme. In Appendix C, we provide a detailed explanation on how the average matrix  $\widehat{A}_{i,j+1/2}$  and the corresponding matrices  $R_{i,j+\frac{1}{2}}$  and  $R_{i,j+\frac{1}{2}}^{-1}$  are computed for the 1-D isentropic Euler system (5.2)–(5.3).

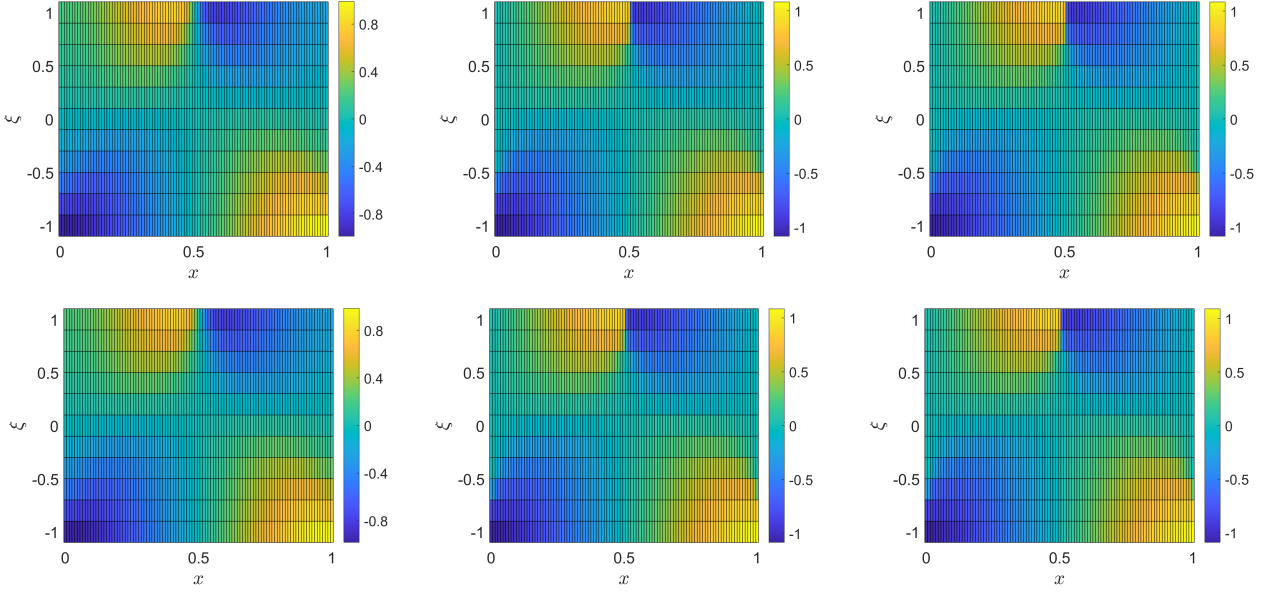


Figure 5.2: Example 1: Numerical results computed by the 1- (left column), 2- (middle column), and 5-Order (top row) collocation (top row) and YM (bottom row) schemes.

**Example 2.** In this example taken from [12], we consider the isentropic Euler system (5.2)–(5.3) with the following initial conditions:

$$(\rho, q)(x, \xi, 0) = \begin{cases} \mathbf{u}_L, & \text{if } x < 0 \\ \mathbf{u}\left(\frac{1}{2}\xi + \mathbf{u}_L; \mathbf{u}_L\right), & \text{otherwise,} \end{cases}$$

where  $\mathbf{u}_L = (1, 1)^\top$ , prescribed in the computational domain  $[-1, 1] \times [-1, 1]$  subject to the free boundary conditions. In Figure 5.3, we plot the initial data for both  $\rho$  and  $q$ .

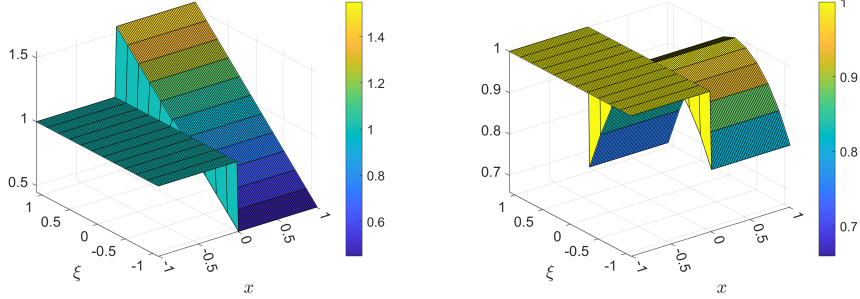


Figure 5.3: Example 2: Initial data for  $\rho$  (left) and  $q$  (right).

We compute the numerical solutions until the final time  $t = 0.25$  by the studied 1-, 2-, and 5-Order YM schemes on the uniform mesh with  $N_x = 100$ ,  $N_\xi = 10$ . For the discretization in phase space  $\mathbf{u} = (\rho, q)$ , we set  $[0.3, 1.8] \times [0.3, 1.3]$  and use  $N_u = 25$  in for each variable. We present the results computed by the collocation and YM approaches in Figures 5.4 and 5.5, where the solution exhibits a shock wave for  $\xi < 0$  in the first family and a rarefaction wave of the first family for all values of  $\xi \geq 0$ . One can clearly see that the solutions computed by the collocation and YM methods are the same and the improvements of resolution in the numerical results computed by the high-order schemes, particularly near the shock waves.

As mentioned in Remarks 3.1 and 4.2, one can also use the numerical fluxes defined in (3.7)–(3.8), and the obtained numerical results coincide with those computed by the numerical fluxes given by (3.2). In Figure 5.6, we plot the numerical results computed by the fluxes in (3.7)–(3.8), where it can clearly see that the computed results are the same as those plotted in Figures 5.4 and 5.5.

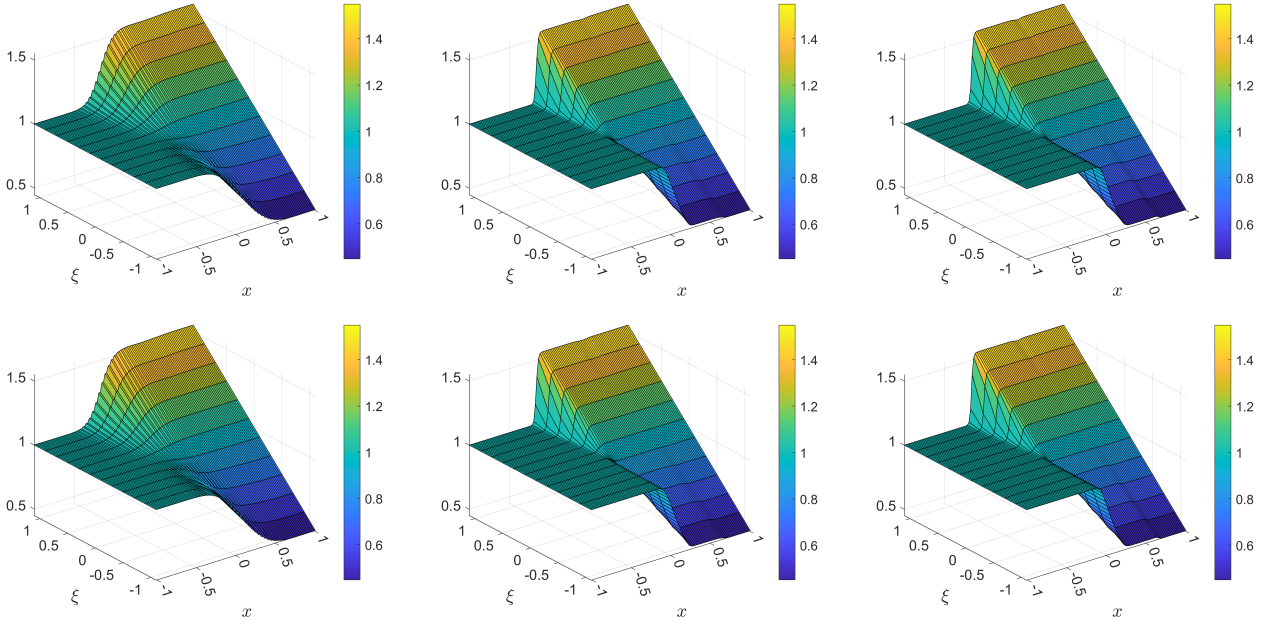


Figure 5.4: Example 2: Numerical results of  $\rho$  computed by the 1- (left column), 2- (middle column), and 5-Order (right column) collocation (top row) and YM (bottom row) schemes.

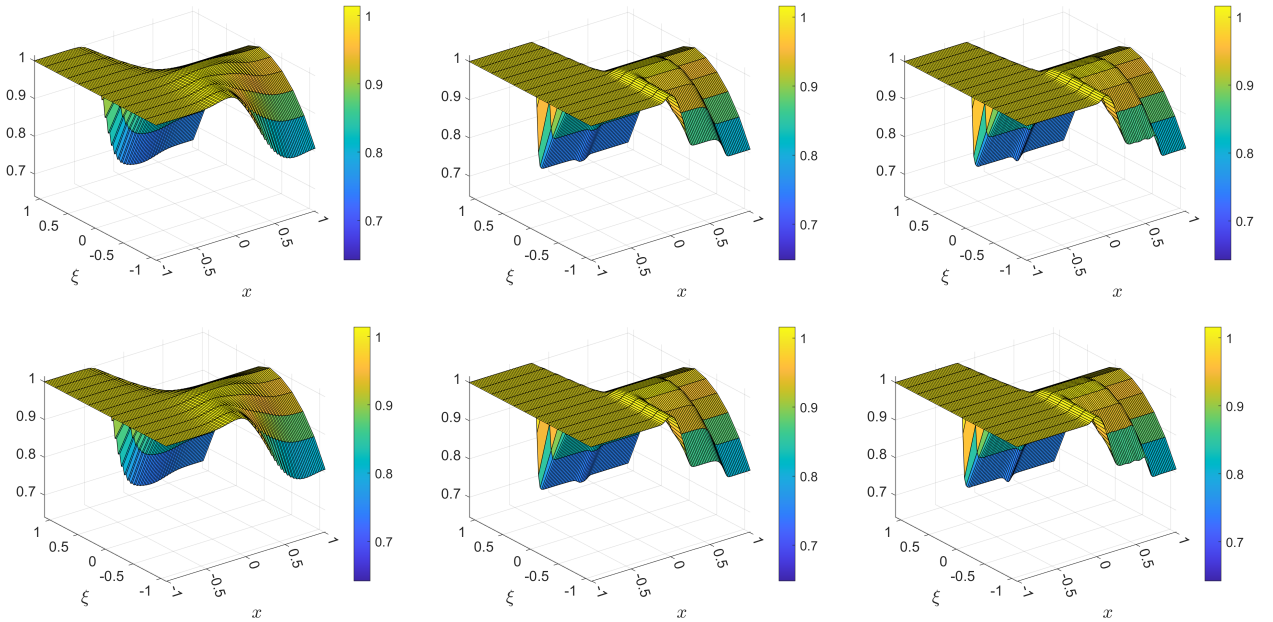


Figure 5.5: Example 2: Numerical results of  $q$  computed by the 1- (left column), 2- (middle column), and 5-Order (right column) collocation (top row) and YM (bottom row) schemes.

**Example 3.** In this example, we consider the isentropic Euler system (5.2)–(5.3) with the following initial conditions:

$$\mathbf{u}(x, \xi, 0) = \begin{cases} (0.4 + 0.1\xi, 1.2), & \text{if } x < -0.3, \\ (0.4, 1.0), & \text{otherwise,} \end{cases}$$

prescribed in the computational domain  $[-1, 1] \times [-1, 1]$  subject to the free boundary conditions. In Figure 5.7, we plot the initial data for both  $\rho$  and  $q$ .

We compute the numerical solutions until the final time  $t = 0.2$  by the studied 1-, 2-, and 5-Order schemes on the uniform mesh with  $N_x = 100$ ,  $N_\xi = 10$ . For the discretization in phase space  $\mathbf{u} = (\rho, q)$ , we set  $[0.05, 1] \times [0.3, 2.5]$  and use  $N_{\mathbf{u}} = 20$  in for each variable. The obtained numerical

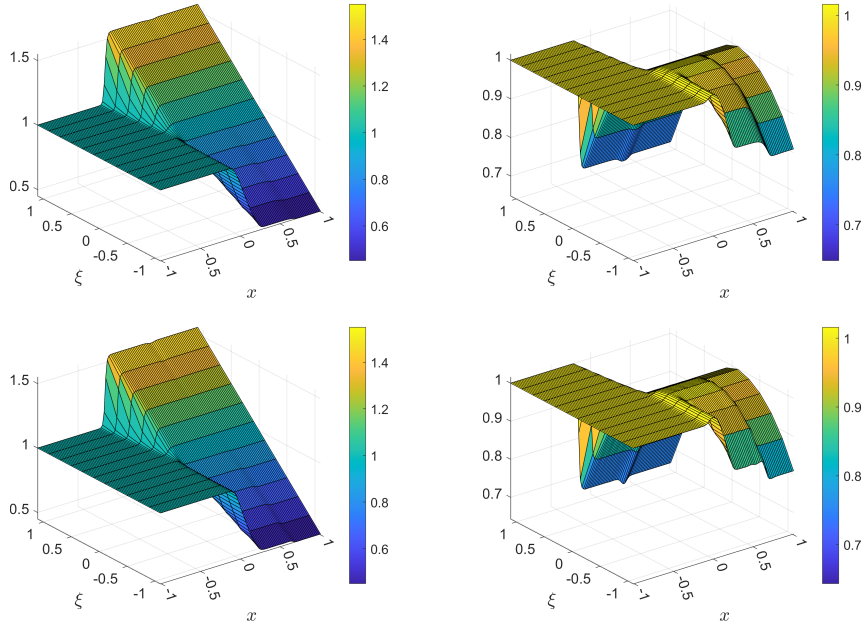


Figure 5.6: Example 2: Numerical results of  $\rho$  (left column) and  $q$  (right column) computed by the 2- (top row), and 5-Order (bottom row) YM schemes by the numerical fluxes defined in (3.7)–(3.8).

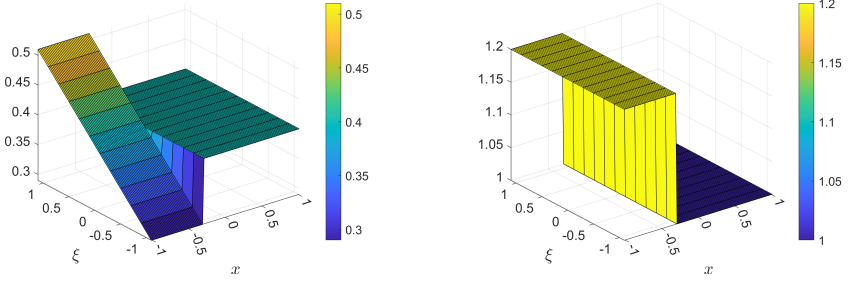


Figure 5.7: Example 3: Initial data for  $\rho$  (left) and  $q$  (right).

results are presented in Figures 5.8 and 5.9, where one can see that, for both the collocation and YM methods, the resolutions of the results computed by the 2-Order scheme are much better than the 1-Order counterpart, and the 5-Order scheme achieves the best resolutions, demonstrating a substantial difference in the resolution when using higher-order schemes.

## 5.2 Numerical Examples for Deterministic Hyperbolic Conservation Laws

In this section, we apply the studied YM and collocation schemes to several numerical examples of deterministic hyperbolic conservation laws, including conservation laws with discontinuous fluxes, the pressureless gas dynamics system, and the Burgers equation with non-atomic support. The YM formulation enables the use of different objectives in the reconstruction step. For conservation laws with discontinuous coefficients, the particular choice of entropy determines the selection of different solutions.

### 5.2.1 Conservation Laws with Discontinuous Flux

It is instructive to check whether the proposed YM schemes can capture non-unique numerical results on the examples of conservation laws with discontinuous coefficients when taking different entropy functions in the linear programming problem. To this end, we consider the scalar conservation law with a discontinuous flux function:

$$u_t + F(u)_x = 0,$$

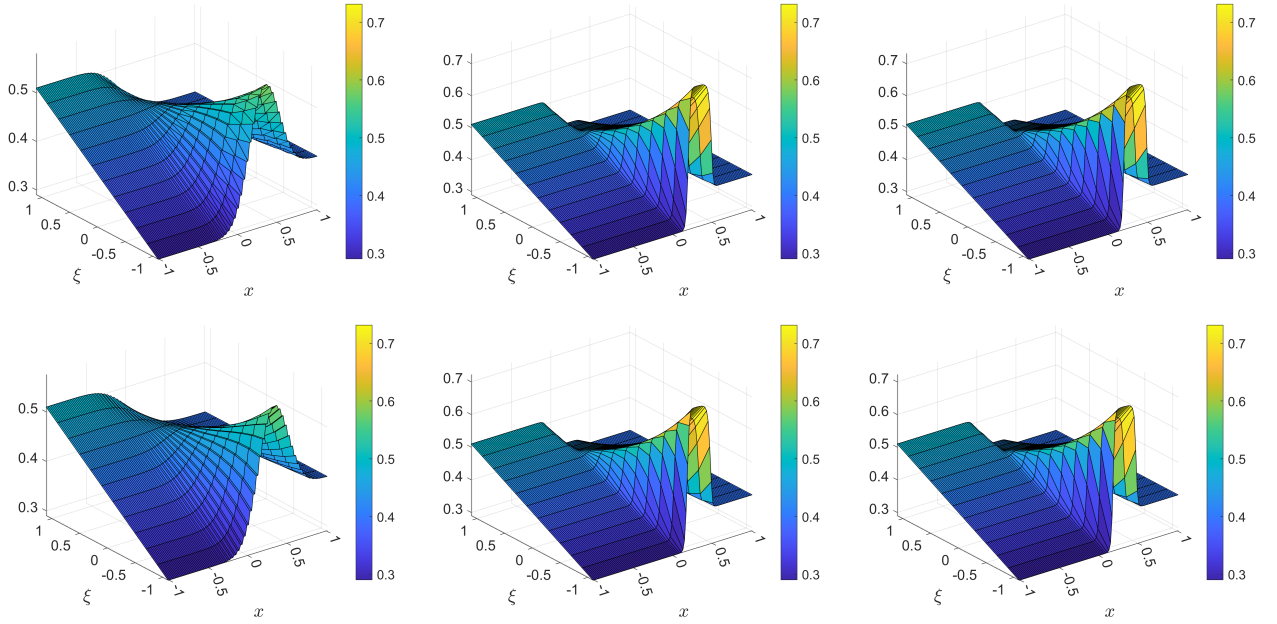


Figure 5.8: Example 3: Numerical results of  $\rho$  computed by the 1- (left column), 2- (middle column), and 5-Order (right column) collocation (top row) and YM (bottom row) schemes.

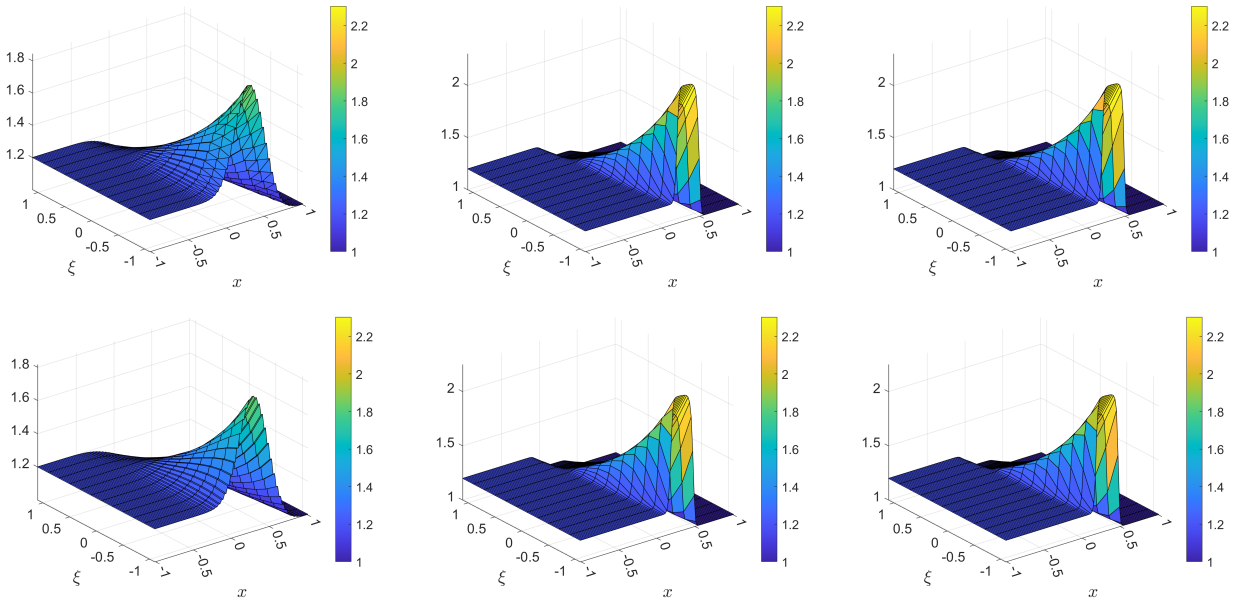


Figure 5.9: Example 3: Numerical results of  $q$  computed by the 1- (left column), 2- (middle column), and 5-Order (right column) collocation (top row) and YM (bottom row) schemes.

where  $F(u) = (1 - H(x))g(u) + H(x)f(u)$ , and  $H(x)$  is the heaviside function. We refer the readers to [45] for more details.

**Example 4.** In this example taken from [45], we take

$$g(u) = u(1 - u), \quad f(u) = 1.1u(1 - u),$$

and consider the following initial data:

$$u(x, \xi, 0) = \begin{cases} 0.65, & \text{if } x < 0 \\ 0.35, & \text{otherwise,} \end{cases}$$

prescribed in the computational domain  $[-4, 4]$  subject to the free boundary conditions. The corresponding entropy functions  $\eta$  in (2.2a) are  $\eta(u) = \frac{1}{2}u^2$  and  $\eta(u) = |u - c|$ , where  $c$  is a constant satisfying  $c \in [u_{\min}, u_{\max}]$ .

We compute the numerical solutions until the final time  $t = 2$  by the studied 1-, 2-, and 5-Order schemes on the uniform mesh with  $N_x = 100$ ,  $N_\xi = 1$ . For the discretization in phase space, we set  $u \in [-1, 1]$  and use  $N_u = 50$ . We plot the obtained numerical results in Figure 5.10, where one can see that the numerical results computed by the studied YM schemes are different when utilizing different entropy functions. The obtained results are in a good agreement with the numerical results reported in [45], where varied schemes are used to produce different numerical solutions. We also present the corresponding moments and supports of the YM in Figures 5.11–5.12. One can notice that the moments and supports of the YM also vary when different entropy functions are utilized.

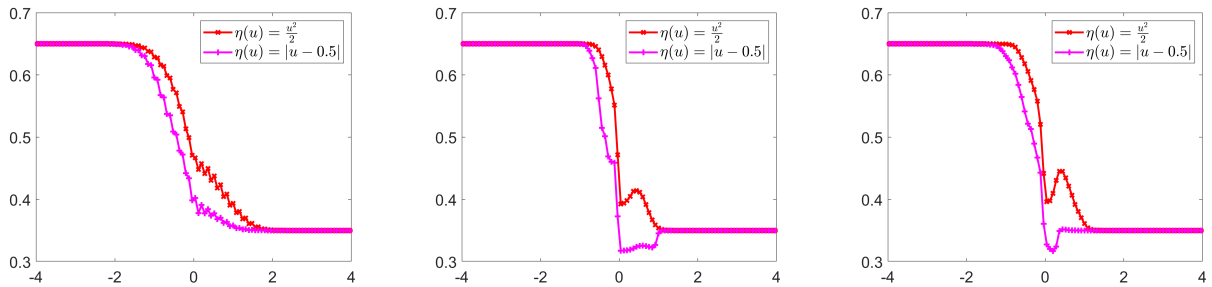


Figure 5.10: Example 4: Numerical results computed by the 1- (left), 2-(middle), and 5-Order (right) collocation and YM methods with  $\eta(u) = \frac{1}{2}u^2$  and  $\eta(u) = |u - 0.5|$ .

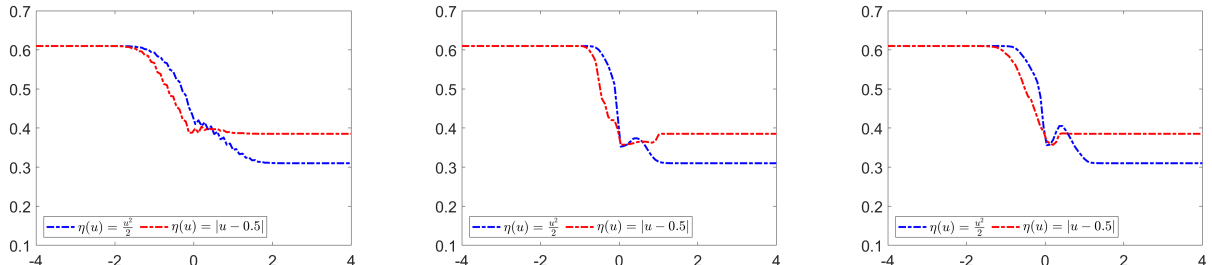


Figure 5.11: Example 4: Moments computed by the 1- (left), 2-(middle), and 5-Order (right) YM methods at the final time  $t = 2$  with  $\eta(u) = \frac{1}{2}u^2$  and  $\eta(u) = |u - 0.5|$ .

**Example 5.** In this example taken from [45], we take

$$g(u) = \frac{2u(1-u)}{1+u}, \quad f(u) = \frac{2u(1-u)}{2-u},$$

and consider the following initial data:

$$u(x, \xi, 0) = 0.5,$$

prescribed in the computational domain  $[-4, 4]$  subject to the free boundary conditions. The corresponding entropy functions  $\eta$  in (2.2a) are  $\eta(u) = \frac{1}{2}u^2$  and  $\eta(u) = |u - 0.5|$ .

We compute the numerical solutions until the final time  $t = 3$  by the studied 1-, 2-, and 5-Order schemes on the uniform mesh with  $N_x = 100$ ,  $N_\xi = 1$ . For the discretization in phase space, we set  $u \in [-1, 1]$  and use  $N_u = 50$ . The obtained numerical results are presented in Figures 5.13–5.15, and one can see that, as in the previous example, the considered YM schemes can produce non-unique solution when different entropy functions are employed.

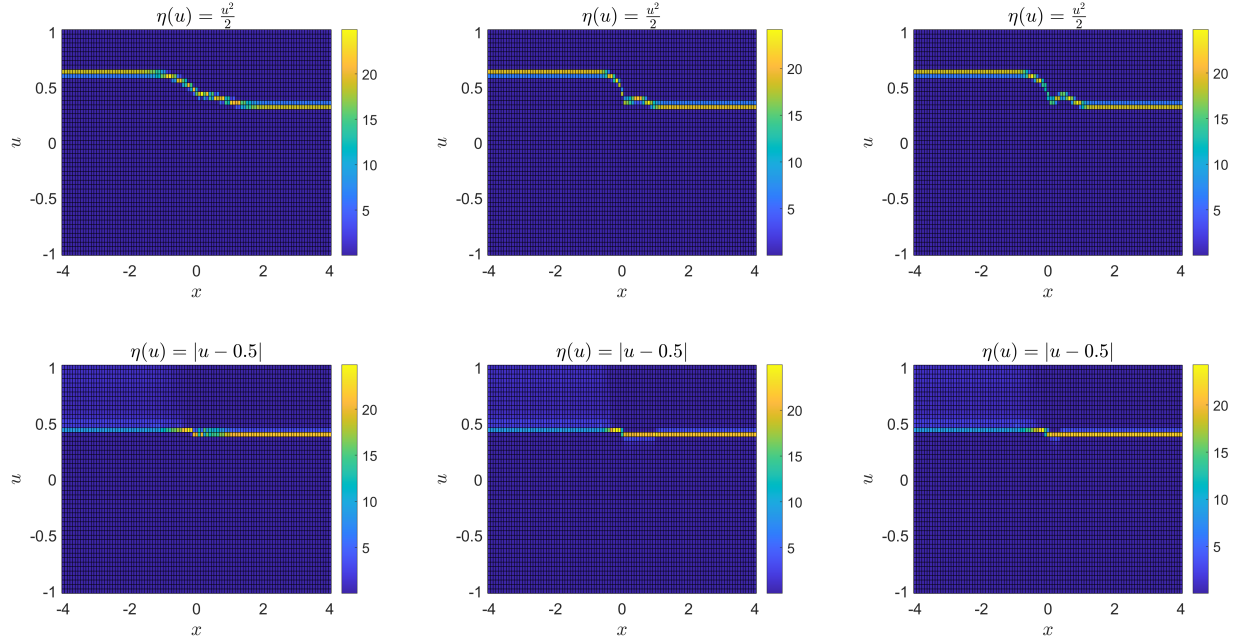


Figure 5.12: Example 4: Supports of the YM computed by the 1- (left column), 2-(middle column), and 5-Order (right column) YM method at the final time  $t = 2$  with  $\eta(u) = \frac{1}{2}u^2$  (top row) and  $\eta(u) = |u - 0.5|$  (bottom row).

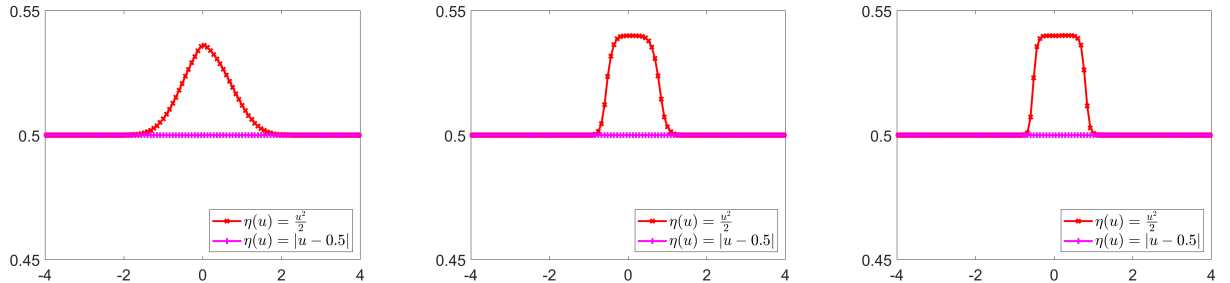


Figure 5.13: Example 5: Numerical results computed by the 1- (left), 2-(middle), and 5-Order (right) collocation and YM methods with  $\eta(u) = \frac{1}{2}u^2$  and  $\eta(u) = |u - 0.5|$ .

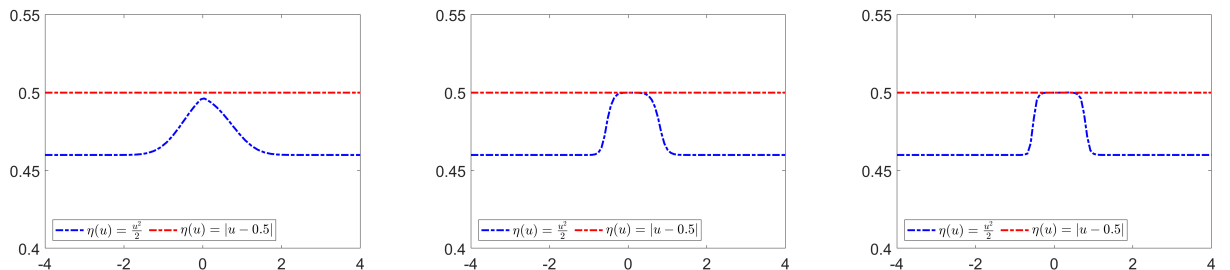


Figure 5.14: Example 5: Moments computed by the 1- (left), 2-(middle), and 5-Order (right) YM methods at the final time  $t = 3$  with  $\eta(u) = \frac{1}{2}u^2$  and  $\eta(u) = |u - 0.5|$ .

**Remark 5.2** In the case of discontinuous fluxes, the expected distinct solutions are obtained simply by modifying the objective function in the linear programming formulation. Examples 4 and 5 demonstrate that the YM formulation can serve as a selection criterion for the corresponding solutions.

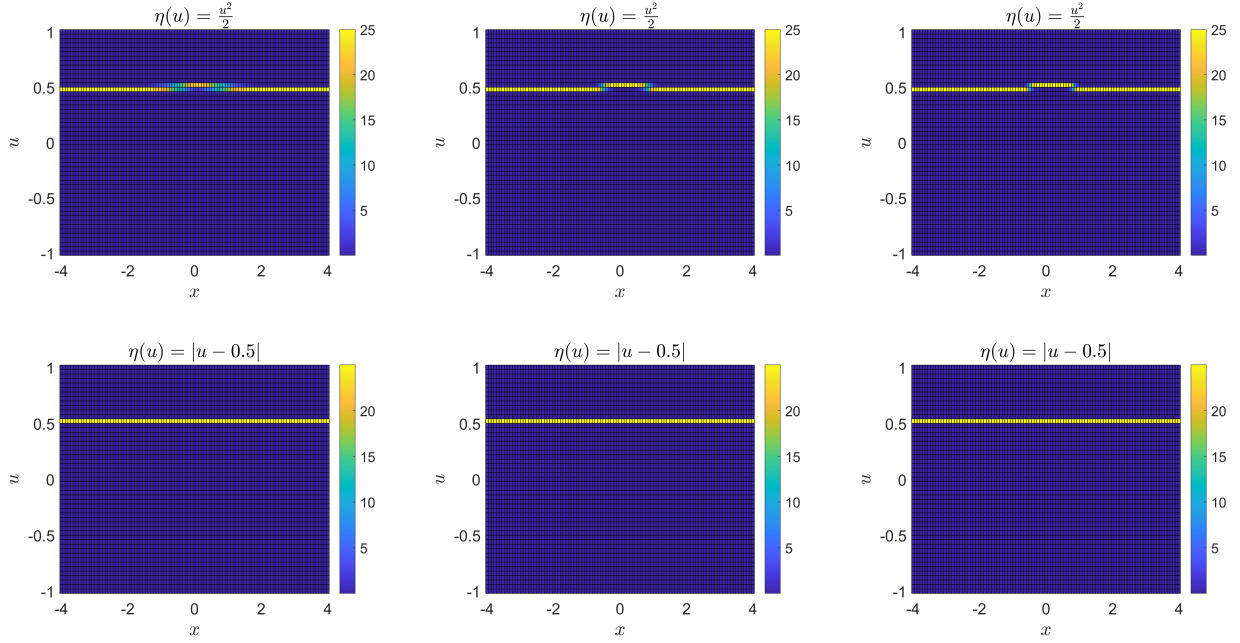


Figure 5.15: Example 5: Supports obtained by the 1- (left column), 2-(middle column), and 5-Order (right column) YM method at the final time  $t = 3$  with  $\eta(u) = \frac{1}{2}u^2$  (top row) and  $\eta(u) = |u - 0.5|$  (bottom row).

### 5.2.2 Pressureless Gas Dynamics System

In this section, we consider the 1-D pressureless gas dynamics system, which reads as

$$\begin{cases} \rho_t + q_x = 0, \\ q_t + \left(\frac{q^2}{\rho}\right)_x = 0, \end{cases} \quad (5.4)$$

where  $\rho$  and  $v := \frac{q}{\rho}$  are the density and velocity, respectively. The corresponding entropy function  $\eta$  in (2.2a) is defined by  $\eta = \frac{1}{2}\rho v^2$ .

It should be noted that the 1-D pressureless gas dynamics system is weakly hyperbolic and its solutions develop delta-shocks and vacuum states in finite time, which make the design of stable and accurate numerical methods very challenging.

**Example 6.** In the last example, we consider the pressureless gas dynamics system (5.4) and take the following initial data:

$$\mathbf{u}(x, \xi, 0) = \begin{cases} (1, 2), & \text{if } x < -0.5 \\ (1, 0), & \text{otherwise,} \end{cases}$$

prescribed in the computational domain  $[-1, 1]$  subject to the free boundary conditions. We note that a peak will be formed at later time  $t > 0$  in the computed  $\rho$  and  $q$ . In the numerical results, a delta-shock will be formed at later time.

We compute the numerical solutions until the final time  $t = 1$  by the studied 1-, 2-, and 5-Order YM schemes on the uniform mesh with  $N_x = 50$ ,  $N_\xi = 1$ . For the discretization in phase space  $\mathbf{u} = (\rho, q)$ , we use  $[0.2, 8] \times [-0.3, 8]$  with  $N_u = 200$ ,  $[0.2, 25] \times [-0.3, 25]$  with  $N_u = 300$ , and  $[0.2, 30] \times [-0.3, 30]$  with  $N_u = 300$  for each variable in the 1-, 2-, and 5-Order schemes, respectively. The obtained numerical results are presented in Figure 5.16, where one can see that, the higher-order schemes produce much sharper delta-shocks than the 1-Order counterpart, which demonstrates that the robustness of the studied YM scheme.

To further investigate, we also compute numerical results using the first-order scheme on a uniform mesh with  $N_x = 50$ ,  $N_\xi = 1$ , and set  $[0.2, 20] \times [-0.3, 20]$  with  $N_u = 300$  for the discretization in phase

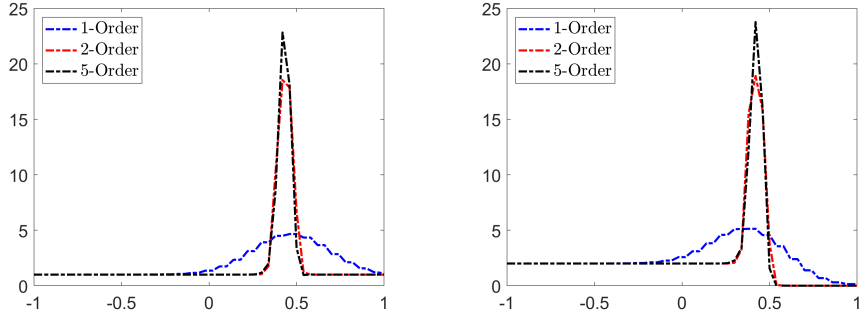


Figure 5.16: Example 6: Numerical results of  $\rho$  (left) and  $q$  (right) computed by the 1-, 2-, and 5-Order YM schemes.

space  $\mathbf{u} = (\rho, q)$ . The obtained numerical results are presented in Figure 5.17. As observed, both the YM and collocation schemes capture sharper delta-shocks; however, the resolution is still inferior to that obtained by the 2- and 5-Order schemes, even on a finer mesh. These results highlight the superior efficiency of higher-order schemes. At the same time, we also present the moment  $\iint_{\mathbb{R} \times \mathbb{R}} \rho d\mu(\rho, q)$  and  $\iint_{\mathbb{R} \times \mathbb{R}} q d\mu(\rho, q)$ , and the marginal with respect to  $\rho$  and  $q$ , respectively, i.e.,  $\tilde{\rho} = \int_{\mathbb{R}} \mu^*(\rho, q) dq$  and  $\tilde{q} = \int_{\mathbb{R}} \mu^*(\rho, q) d\rho$ ; see Figures 5.18–5.19.

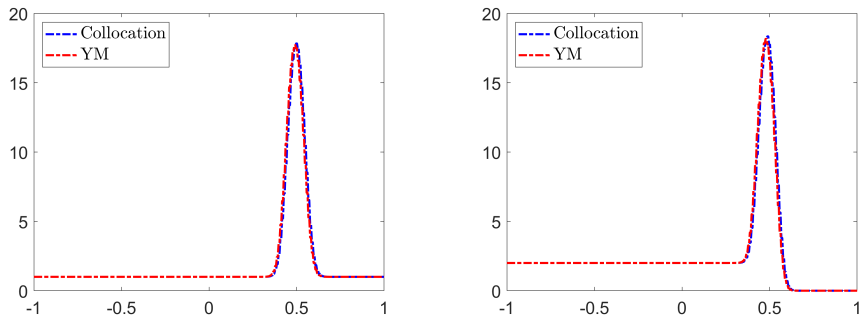


Figure 5.17: Example 6: Numerical results of  $\rho$  (left) and  $q$  (right) computed by the 1-Order collocation and YM schemes.

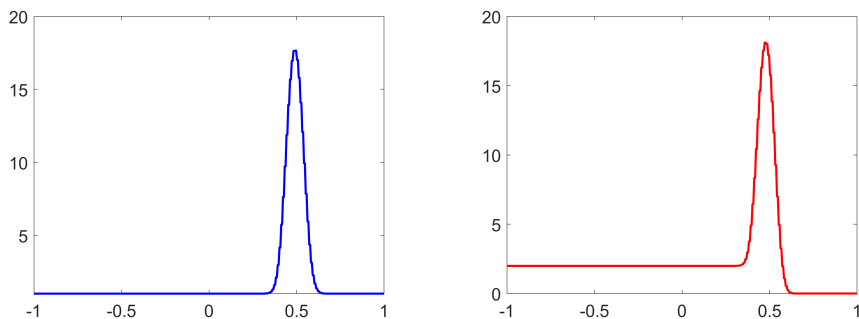


Figure 5.18: Example 6: Moment of  $\rho$  (left) and  $q$  (right) computed by the 1-Order YM scheme.

### 5.2.3 Burgers Equation with Non-Atomic Support

In the last section, we consider an example taken from [27] (see also [12]), where the YM may have non-atomic support. We set the factor  $\lambda_F$  in (2.2c) to 0.05. By modifying the upper bound on the weights of the YM, we eliminate the atomic solution, compelling the linear programming solver to construct a different YM. This slight adjustment enables us to recover a solution that is consistent with the one presented in [27].

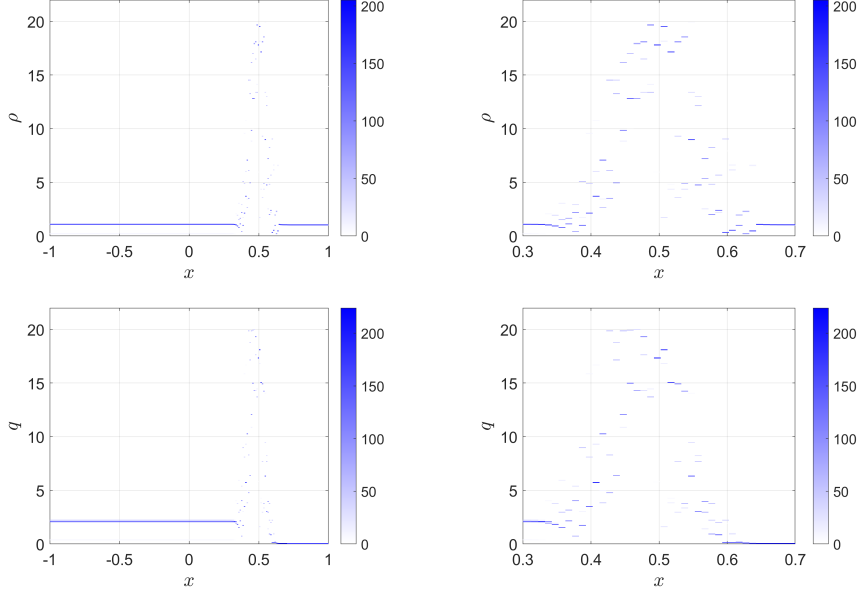


Figure 5.19: Example 6:  $\tilde{\rho}$  (top row) and  $\tilde{q}$  (bottom row) and zoom at  $x \in [0.3, 0.7]$  computed by the 1-Order YM scheme.

**Example 7.** In the last example, we consider the following initial data

$$u_0(x, \xi) = \begin{cases} 1.5 & \text{if } x < 0.5 \\ 0.5 & \text{otherwise,} \end{cases}$$

subject to the free boundary conditions imposed in the computational domain  $[-1, 1]$ . In Figure 5.20, we plot the support of the YM at the initial time.

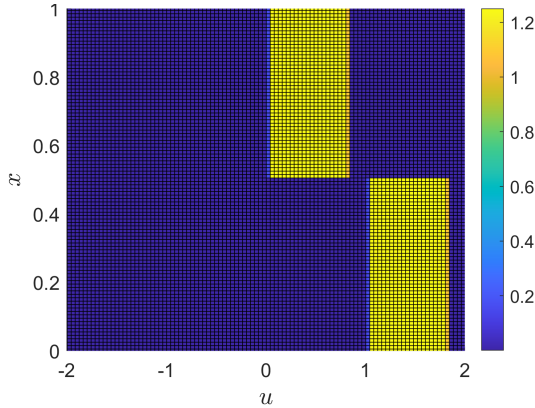


Figure 5.20: Example 7: Support of YM at the initial time.

We compute the numerical results until the final time  $t = 0.25$  by the studied 1-, 2-, and 5-Order schemes on the uniform mesh with  $N_x = 100$  and  $N_\xi = 1$ . The phase space is confined to the interval  $u \in [-2, 2]$  and is uniformly discretized into  $N_u = 100$  equidistant cells. The obtained numerical results are presented in Figure 5.21, where one can clearly see that the measure with non-atomic support can be captured by our linear programming algorithm if we choose  $\lambda_F \neq 1$ , and in contrast to Example 1, the support of the YM solution is distributed rather than concentrated. At the same time, the use of higher-order schemes yields a significantly sharper resolution.

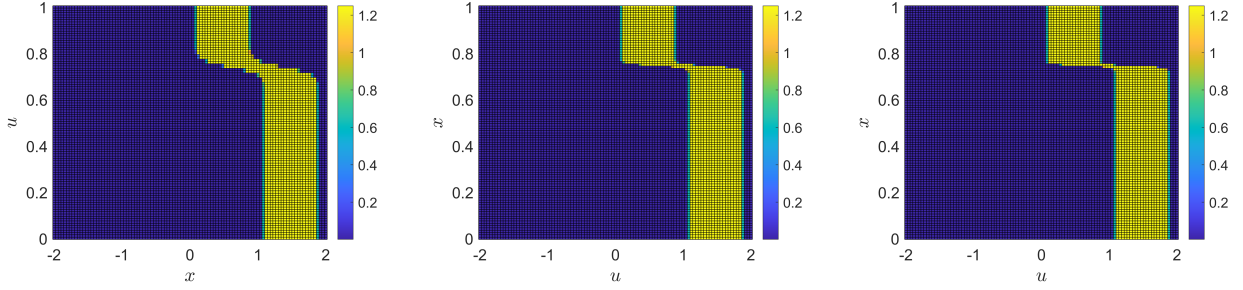


Figure 5.21: Example 7: Support of YM computed by the 1- (left), 2- (middle), and 5-Order (right) schemes at the final time  $t = 0.25$ .

## 6 Conclusions

In this paper, we extended the existing first-order scheme for solving random hyperbolic conservation laws using linear programming to higher-order ones. We first extended the first-order scheme to second-order by employing piecewise linear reconstruction and then to fifth order of accuracy in the framework of finite-difference A-WENO scheme. These extensions enhance the resolution of discontinuities while preserving structure-preserving properties. We validated the proposed methods through a series of random and deterministic hyperbolic conservation laws, including the one-dimensional Burgers equation, isentropic system, the scalar conservation law with a discontinuous flux function, pressureless gas dynamics system, and Burgers equation with non-atomic support. The obtained numerical results demonstrate that higher-order schemes significantly improve the resolution of complex wave structures and reduce numerical dissipation, particularly near shock and rarefaction waves. Future work includes extending these approaches to (nonconservative) multi-dimensional random hyperbolic problems, improving computational efficiency via adaptive refinement strategies.

### Declarations:

**Acknowledgments.** The authors would like to thank Giuseppe Coclite (Politecnico di Bari, Italy) for providing the idea of the example on the discontinuous flux as well as interesting discussions on the topic.

The work of S. Chu was supported in part by the DFG (German Research Foundation) through HE5386/19-3, 27-1. The work of M. Herty was funded by the DFG–SPP 2183: Eigenschaftsgeregelte Umformprozesse with the Project(s) HE5386/19-2,19-3 Entwicklung eines flexiblen isothermen Reckschmiedeprozesses für die eigenschaftsgeregelte Herstellung von Turbinenschaufeln aus Hochtemperaturwerkstoffen (424334423) and by the Deutsche Forschungsgemeinschaft (DFG, German Research Foundation)–SPP 2410 Hyperbolic Balance Laws in Fluid Mechanics: Complexity, Scales, Randomness (CoScaRa) within the Project(s) HE5386/26-1 (Numerische Verfahren für gekoppelte Mehrskalenprobleme, 525842915) and (Zufällige kompressible Euler Gleichungen: Numerik und ihre Analysis, 525853336) HE5386/27-1.

**Conflicts of interest.** On behalf of all authors, the corresponding author states that there is no conflict of interest.

**Data and software availability.** The data that support the findings of this study and MATLAB codes developed by the authors and used to obtain all of the presented numerical results are available by the corresponding author upon request.

## A 1-D Local Characteristic Decomposition Based Piecewise Linear Interpolant

In this appendix, we briefly describe the 1-D local characteristic decomposition (LCD) based piecewise linear interpolant.

In order to suppress the oscillations in the piecewise linear reconstruction (3.3)–(3.6), we apply the generalized minmod limiter to the local characteristic variables. To this end, we first introduce the matrix  $\hat{A}_{i,j+\frac{1}{2}} = A(\hat{\mathbf{u}}_{i,j+\frac{1}{2}})$ , where  $A = \frac{\partial \mathbf{f}}{\partial \mathbf{u}}$  is the Jacobian and  $\hat{\mathbf{u}}_{i,j+\frac{1}{2}}$  is either a simple average  $(\mathbf{u}_{i,j} + \mathbf{u}_{i,j+1})/2$  or another type of average of the  $\mathbf{u}_{i,j}$  and  $\mathbf{u}_{i,j+1}$  states.

We then compute the matrices  $R_{i,j+\frac{1}{2}}$  and  $R_{i,j+\frac{1}{2}}^{-1}$  such that  $R_{i,j+\frac{1}{2}} \hat{A}_{i,j+\frac{1}{2}} R_{i,j+\frac{1}{2}}^{-1}$  is a diagonal matrix and introduce the local characteristic variables  $\boldsymbol{\Gamma}_k$  in the neighborhood of  $x = x_{j+\frac{1}{2}}$ :

$$\boldsymbol{\Gamma}_k = R_{i,j+\frac{1}{2}}^{-1} \mathbf{u}_{i,k}, \quad k = j-1, \dots, j+2.$$

Equipped with the values  $\boldsymbol{\Gamma}_{i,j-1}$ ,  $\boldsymbol{\Gamma}_{i,j}$ ,  $\boldsymbol{\Gamma}_{i,j+1}$ , and  $\boldsymbol{\Gamma}_{i,j+2}$ , we reconstruct  $\boldsymbol{\Gamma}$  by computing

$$(\boldsymbol{\Gamma}_x)_{i,j} = \text{minmod} \left( \theta \frac{\boldsymbol{\Gamma}_{i,j} - \boldsymbol{\Gamma}_{i,j-1}}{\Delta x}, \frac{\boldsymbol{\Gamma}_{i,j+1} - \boldsymbol{\Gamma}_{i,j-1}}{2\Delta x}, \theta \frac{\boldsymbol{\Gamma}_{i,j+1} - \boldsymbol{\Gamma}_{i,j}}{\Delta x} \right),$$

and

$$(\boldsymbol{\Gamma}_x)_{i,j+1} = \text{minmod} \left( \theta \frac{\boldsymbol{\Gamma}_{i,j+1} - \boldsymbol{\Gamma}_{i,j}}{\Delta x}, \frac{\boldsymbol{\Gamma}_{i,j+2} - \boldsymbol{\Gamma}_{i,j}}{2\Delta x}, \theta \frac{\boldsymbol{\Gamma}_{i,j+2} - \boldsymbol{\Gamma}_{i,j+1}}{\Delta x} \right),$$

where the minmod function is defined by (3.6). After that, we evaluate

$$\boldsymbol{\Gamma}_{i,j+\frac{1}{2}}^- = \boldsymbol{\Gamma}_{i,j} + \frac{\Delta x}{2} (\boldsymbol{\Gamma}_x)_{i,j} \quad \text{and} \quad \boldsymbol{\Gamma}_{i,j+\frac{1}{2}}^+ = \boldsymbol{\Gamma}_{i,j+1} - \frac{\Delta x}{2} (\boldsymbol{\Gamma}_x)_{i,j+1}.$$

Finally, one can obtain the corresponding point values of  $\mathbf{u}$  by

$$\mathbf{u}_{i,j+\frac{1}{2}}^- = R_{i,j+\frac{1}{2}} \boldsymbol{\Gamma}_{i,j+\frac{1}{2}}^- \quad \text{and} \quad \mathbf{u}_{i,j+\frac{1}{2}}^+ = R_{i,j+\frac{1}{2}} \boldsymbol{\Gamma}_{i,j+\frac{1}{2}}^+.$$

**Remark A.1** The one-sided point values of  $\mathbf{u}_{i,j+\frac{1}{2}}^{\pm,*}$  can be computed in the same manner by using  $\mathbf{u}_{i,j}^*$ , and here we omit it for the sake of brevity.

## B 1-D Local Characteristic Decomposition Based Fifth-Order WENO-Z Interpolant

In this appendix, we briefly describe the 1-D LCD based fifth-order WENO-Z interpolant.

Given the point values  $\mathbf{u}_{i,j}$ , for the  $k$ -th component of  $\mathbf{u}_{i,j}$ , the value  $u_{i,j+\frac{1}{2}}^{(k),-}$  is computed using a weighted average of the three parabolic interpolants  $\mathcal{P}_0(x)$ ,  $\mathcal{P}_1(x)$ , and  $\mathcal{P}_2(x)$  obtained using the stencils  $[x_{j-2}, x_{j-1}, x_j]$ ,  $[x_{j-1}, x_j, x_{j+1}]$ , and  $[x_j, x_{j+1}, x_{j+2}]$ , respectively:

$$u_{i,j+\frac{1}{2}}^{(k),-} = \sum_{k=0}^2 \omega_k \mathcal{P}_k(x_{j+\frac{1}{2}}), \tag{B.1}$$

where

$$\begin{aligned} \mathcal{P}_0(x_{j+\frac{1}{2}}) &= \frac{3}{8} u_{i,j-2}^{(k)} - \frac{5}{4} u_{i,j-1}^{(k)} + \frac{15}{8} u_{i,j}^{(k)}, \\ \mathcal{P}_1(x_{j+\frac{1}{2}}) &= -\frac{1}{8} u_{i,j-1}^{(k)} + \frac{3}{4} u_{i,j}^{(k)} + \frac{3}{8} u_{i,j+1}^{(k)}, \\ \mathcal{P}_2(x_{j+\frac{1}{2}}) &= \frac{3}{8} u_{i,j}^{(k)} + \frac{3}{4} u_{i,j+1}^{(k)} - \frac{1}{8} u_{i,j+2}^{(k)}. \end{aligned} \tag{B.2}$$

In order to ensure (B.1)–(B.2) is fifth-order accurate and non-oscillatory, one can take the weights  $\omega_\ell^{(k)}$  in (B.1) to be

$$\omega_\ell^{(k)} := \frac{\alpha_\ell}{\alpha_0 + \alpha_1 + \alpha_2}, \quad \alpha_\ell = d_k \left[ 1 + \left( \frac{\tau_5}{\beta_\ell + \varepsilon} \right)^p \right], \quad \tau_5 = |\beta_2 - \beta_0|, \quad (\text{B.3})$$

where  $d_0 = \frac{1}{16}$ ,  $d_1 = \frac{5}{8}$ , and  $d_2 = \frac{5}{16}$ , and the smoothness indicators  $\beta_k$  in (B.3) are given by

$$\begin{aligned} \beta_0 &= \frac{13}{12} (u_{i,j-2}^{(k)} - 2u_{i,j-1}^{(k)} + u_{i,j}^{(k)})^2 + \frac{1}{4} (u_{i,j-2}^{(k)} - 4u_{i,j-1}^{(k)} + 3u_{i,j}^{(k)})^2, \\ \beta_1 &= \frac{13}{12} (u_{i,j-1}^{(k)} - 2u_{i,j}^{(k)} + u_{i,j+1}^{(k)})^2 + \frac{1}{4} (u_{i,j-1}^{(k)} - u_{i,j+1}^{(k)})^2, \\ \beta_2 &= \frac{13}{12} (u_{i,j}^{(k)} - 2u_{i,j+1}^{(k)} + u_{i,j+2}^{(k)})^2 + \frac{1}{4} (3u_{i,j}^{(k)} - 4u_{i,j+1}^{(k)} + u_{i,j+2}^{(k)})^2. \end{aligned} \quad (\text{B.4})$$

In all of the numerical examples reported in this paper, we have used  $p = 2$  and  $\varepsilon = 10^{-12}$ . The corresponding right-sided value  $u_{i,j+\frac{1}{2}}^{(k),+}$  can also be derived using a mirror-symmetric approach, and here we omit it for the sake of brevity.

As in Appendix A, to ensure the nonoscillatory nature of the reconstruction (B.1)–(B.4), we also need to adopt the reconstruction procedure within the LCD framework. To this end, with the matrices  $R_{i,j+\frac{1}{2}}$  and  $R_{i,j+\frac{1}{2}}^{-1}$  (see Appendix C), we first introduce the local characteristic variables in the neighborhood of  $x = x_{j+\frac{1}{2}}$ :

$$\Gamma_{i,\ell}^{(k)} = R_{i,j+\frac{1}{2}}^{-1} u_{i,\ell}^{(k)}, \quad \ell = j-2, \dots, j+3.$$

Equipped with the values  $\Gamma_{i,j-2}^{(k)}$ ,  $\Gamma_{i,j-1}^{(k)}$ ,  $\Gamma_{i,j}^{(k)}$ ,  $\Gamma_{i,j+1}^{(k)}$ ,  $\Gamma_{i,j+2}^{(k)}$ , and  $\Gamma_{i,j+3}^{(k)}$ , we then apply the interpolation procedure (B.1)–(B.4) to  $\Gamma$  and obtain  $\Gamma_{i,j+\frac{1}{2}}^{(k),-}$  (the values of  $\Gamma_{i,j+\frac{1}{2}}^{(k),+}$  are computed in the mirror-symmetric way). Finally, the corresponding one-sided point values of  $u_{i,j+\frac{1}{2}}^{(k),-}$  are given by

$$u_{i,j+\frac{1}{2}}^{(k),-} = R_{i,j+\frac{1}{2}} \Gamma_{i,j+\frac{1}{2}}^{(k),-}.$$

**Remark B.1** The one-sided point values of  $u_{i,j+\frac{1}{2}}^{\pm,*}$  can be computed in the same manner by using  $u_{i,j}^*$ , and here we omit it for the sake of brevity.

## C Local Characteristic Decomposition Matrices for the 1-D Isentropic Euler System

In this appendix, we introduce how to compute the LCD matrices for the 1-D isentropic Euler system (5.2)–(5.3).

We first compute the Jacobian

$$A(\mathbf{u}) = \frac{\partial \mathbf{f}}{\partial \mathbf{u}} = \begin{pmatrix} 0 & 1 \\ \kappa\gamma\rho^{\gamma-1} - v^2 & 2v \end{pmatrix},$$

and then introduce the matrices

$$\widehat{A}_{i,j+\frac{1}{2}} = \begin{pmatrix} 0 & 1 \\ \kappa\gamma\widehat{\rho}^{\gamma-1} - \widehat{v}^2 & 2\widehat{v} \end{pmatrix},$$

where  $(\hat{\cdot})$  stands for the following averages:

$$\widehat{\rho} = \frac{\rho_{i,j} + \rho_{i,j+1}}{2}, \quad \widehat{v} = \frac{v_{i,j} + v_{i,j+1}}{2},$$

with

$$v_{i,j} = \frac{(\rho v)_{i,j}}{\rho_{i,j}}.$$

Notice that all of the  $(\hat{\cdot})$  quantities have to have a subscript index, that is,  $(\hat{\cdot}) = (\hat{\cdot})_{i,j+\frac{1}{2}}$ , but we omit it for the sake of brevity for all of the quantities except for  $\hat{A}$ . We then compute the matrix  $R_{i,j+\frac{1}{2}}$  composed of the right eigenvectors of  $\hat{A}_{i,j+\frac{1}{2}}$  and obtain

$$R_{i,j+\frac{1}{2}} = \begin{pmatrix} 1 & 1 \\ \hat{v} - \sqrt{\gamma} \hat{\rho}^{(\gamma-1)/2} & \hat{v} + \sqrt{\gamma} \hat{\rho}^{(\gamma-1)/2} \\ 1 & 1 \end{pmatrix} \quad \text{and} \quad R_{i,j+\frac{1}{2}}^{-1} = \begin{pmatrix} \hat{\rho} \hat{v}^2 - \gamma \hat{\rho}^\gamma & 1 - \frac{\hat{\rho}^{(1-\gamma)/2} \hat{v}}{2\sqrt{\gamma}} \\ \frac{2\sqrt{\gamma} \hat{\rho}^{(\gamma+1)/2}}{\hat{\rho}^\gamma - \hat{\rho} \hat{v}^2} & \frac{1}{2} - \frac{2\sqrt{\gamma}}{\hat{\rho}^{(1-\gamma)/2} \hat{v}} \\ \frac{\gamma \hat{\rho}^\gamma - \hat{\rho} \hat{v}^2}{2\sqrt{\gamma} \hat{\rho}^{(\gamma+1)/2}} & \frac{1}{2} + \frac{\hat{\rho}^{(1-\gamma)/2} \hat{v}}{2\sqrt{\gamma}} \end{pmatrix}.$$

## References

- [1] R. ABGRALL AND S. MISHRA, *Uncertainty quantification for hyperbolic systems of conservation laws*, in Handbook of numerical methods for hyperbolic problems, vol. 18 of Handb. Numer. Anal., Elsevier/North-Holland, Amsterdam, 2017, pp. 507–544.
- [2] ADIMURTHI, S. MISHRA, AND G. D. VEERAPPA GOWDA, *Optimal entropy solutions for conservation laws with discontinuous flux-functions*, J. Hyperbolic Differ. Equ., 2 (2005), pp. 783–837.
- [3] T. BARTH, *Non-intrusive uncertainty propagation with error bounds for conservation laws containing discontinuities*, in Uncertainty quantification in computational fluid dynamics, vol. 92 of Lect. Notes Comput. Sci. Eng., Springer, Heidelberg, 2013, pp. 1–57.
- [4] C. BERTHON, M. BREUSS, AND M. TITEUX, *A relaxation scheme for the approximation of the pressureless Euler equations*, Numer. Methods Partial Differential Equations, 22 (2006), pp. 484–505.
- [5] J. P. BOYD, *Chebyshev and Fourier spectral methods*, Dover Publications, Inc., Mineola, NY, second ed., 2001.
- [6] A. BRESSAN, *Hyperbolic systems of conservation laws*, vol. 20 of Oxford Lecture Series in Mathematics and its Applications, Oxford University Press, Oxford, 2000. The one-dimensional Cauchy problem.
- [7] C. CARDOEN, S. MARX, A. NOUY, AND N. SEGUIN, *A moment approach for entropy solutions of parameter-dependent hyperbolic conservation laws*, Numer. Math., 156 (2024), pp. 1289–1324.
- [8] A. CHERTOCK, S. CHU, M. HERTY, A. KURGANOV, AND M. LUKÁČOVÁ-MEDVIĐOVÁ, *Local characteristic decomposition based central-upwind scheme*, J. Comput. Phys., 473 (2023). Paper No. 111718.
- [9] A. CHERTOCK, M. HERTY, A. S. ISKHAKOV, S. JANAJRA, A. KURGANOV, AND M. LUKÁČOVÁ-MEDVIĐOVÁ, *New high-order numerical methods for hyperbolic systems of nonlinear PDEs with uncertainties*, Commun. Appl. Math. Comput., 6 (2024), pp. 2011–2044.
- [10] A. CHERTOCK, M. HERTY, A. KURGANOV, AND M. LUKÁČOVÁ-MEDVIĐOVÁ, *Challenges in Stochastic Galerkin Methods for Nonlinear Hyperbolic Systems with Uncertainty*, to appear: Springer Volume on Advances in Nonlinear Hyperbolic Partial Differential Equations, (2024).
- [11] S. CHU, M. HERTY, AND A. KURGANOV, *Novel local characteristic decomposition based path-conservative central-upwind schemes*, J. Comput. Phys., 524 (2025). Paper No. 113692.

- [12] S. CHU, M. HERTY, M. LUKÁČOVÁ-MEDVIĐOVÁ, AND Y. ZHOU, *Solving random hyperbolic conservation laws using linear programming*. Submitted, preprint is available at <https://arxiv.org/pdf/2501.10104.pdf>.
- [13] S. CHU, M. HERTY, AND E. F. TORO, *High-order flux splitting schemes for the Euler equations of gas dynamics*, Comput. & Fluids, 300 (2025). Paper No. 106738.
- [14] S. CHU AND A. KURGANOV, *Local characteristic decomposition based central-upwind scheme for compressible multifluids*, in Finite volumes for complex applications X. Vol. 2. Hyperbolic and related problems, vol. 433 of Springer Proc. Math. Stat., Springer, Cham, 2023, pp. 73–81.
- [15] S. CHU, A. KURGANOV, AND I. KLIAKHANDLER, *On the gelfand problem and viscosity matrices for two-dimensional hyperbolic systems of conservation laws*, Sib. Electron. Math. Re., 21 (2024), pp. 78–91.
- [16] S. CHU, A. KURGANOV, AND I. MENSHOV, *New adaptive low-dissipation central-upwind schemes*, Appl. Numer. Math., 209 (2025), pp. 155–170.
- [17] S. CHU, A. KURGANOV, AND R. XIN, *A fifth-order A-WENO scheme based on the low-dissipation central-upwind fluxes*, in Hyperbolic Problems: Theory, Numerics, Applications. Vol. II, vol. 35 of SEMA SIMAI Springer Ser., Springer, Cham, 2024, pp. 51–61.
- [18] S. CHU, A. KURGANOV, AND R. XIN, *New more efficient A-WENO schemes*, J. Sci. Comput., 104 (2025). Paper No. 53.
- [19] C. M. DAFERMOS, *Hyperbolic conservation laws in continuum physics*, vol. 325 of Grundlehren der mathematischen Wissenschaften [Fundamental Principles of Mathematical Sciences], Springer-Verlag, Berlin, fourth ed., 2016.
- [20] D. DAI, Y. EPSHTEYN, AND A. NARAYAN, *Hyperbolicity-preserving and well-balanced stochastic Galerkin method for shallow water equations*, SIAM J. Sci. Comput., 43 (2021), pp. A929–A952.
- [21] B. DESPRÉS, G. POËTTE, AND D. LUCOR, *Robust uncertainty propagation in systems of conservation laws with the entropy closure method*, in Uncertainty quantification in computational fluid dynamics, vol. 92 of Lect. Notes Comput. Sci. Eng., Springer, Heidelberg, 2013, pp. 105–149.
- [22] R. J. DiPERNA, *Measure-valued solutions to conservation laws*, Arch. Rational Mech. Anal., 88 (1985), pp. 223–270.
- [23] H. C. ELMAN, C. W. MILLER, E. T. PHIPPS, AND R. S. TUMINARO, *Assessment of collocation and Galerkin approaches to linear diffusion equations with random data*, Int. J. Uncertain. Quantif., 1 (2011), pp. 19–33.
- [24] O. G. ERNST, A. MUGLER, H. STARKLOFF, AND E. ULLMANN, *On the convergence of generalized polynomial chaos expansions*, ESAIM Math. Model. Numer. Anal., 46 (2012), pp. 317–339.
- [25] L. C. EVANS AND R. F. GARIEPY, *Measure theory and fine properties of functions*, Textbooks in Mathematics, CRC Press, Boca Raton, FL, revised ed., 2015.
- [26] H. FEDERER, *Geometric measure theory*, vol. Band 153 of Die Grundlehren der mathematischen Wissenschaften, Springer-Verlag New York, Inc., New York, 1969.
- [27] U. S. FJORDHOLM, R. KÄPPELI, S. MISHRA, AND E. TADMOR, *Construction of approximate entropy measure-valued solutions for hyperbolic systems of conservation laws*, Found. Comput. Math., 17 (2017), pp. 763–827.
- [28] U. S. FJORDHOLM, S. MISHRA, AND E. TADMOR, *On the computation of measure-valued solutions*, Acta Numer., 25 (2016), pp. 567–679.

- [29] Z. GAO, L.-L. FANG, B.-S. WANG, Y. WANG, AND W. S. DON, *Seventh and ninth orders alternative WENO finite difference schemes for hyperbolic conservation laws*, Comput. & Fluids, 202 (2020). Paper No. 104519.
- [30] A. GELB AND E. TADMOR, *Enhanced spectral viscosity approximations for conservation laws*, in Proceedings of the Fourth International Conference on Spectral and High Order Methods (ICOSAHOM 1998) (Herzliya), vol. 33, 2000, pp. 3–21.
- [31] S. GERSTER AND M. HERTY, *Entropies and symmetrization of hyperbolic stochastic Galerkin formulations*, Commun. Comput. Phys., 27 (2020), pp. 639–671.
- [32] S. GERSTER, M. HERTY, AND A. SIKSTEL, *Hyperbolic stochastic Galerkin formulation for the  $p$ -system*, J. Comput. Phys., 395 (2019), pp. 186–204.
- [33] S. GOTTLIEB, D. KETCHESON, AND C.-W. SHU, *Strong stability preserving Runge-Kutta and multistep time discretizations*, World Scientific Publishing Co. Pte. Ltd., Hackensack, NJ, 2011.
- [34] S. GOTTLIEB, C.-W. SHU, AND E. TADMOR, *Strong stability-preserving high-order time discretization methods*, SIAM Rev., 43 (2001), pp. 89–112.
- [35] M. HERTY, A. KOLB, AND S. MÜLLER, *Multiresolution analysis for stochastic hyperbolic conservation laws*, IMA J. Numer. Anal., 44 (2024), pp. 536–575.
- [36] J. S. HESTHAVEN, S. GOTTLIEB, AND D. GOTTLIEB, *Spectral methods for time-dependent problems*, vol. 21 of Cambridge Monographs on Applied and Computational Mathematics, Cambridge University Press, Cambridge, 2007.
- [37] G.-S. JIANG AND C.-W. SHU, *Efficient implementation of weighted ENO schemes*, J. Comput. Phys., 126 (1996), pp. 202–228.
- [38] Y. JIANG, C.-W. SHU, AND M. P. ZHANG, *An alternative formulation of finite difference weighted ENO schemes with Lax-Wendroff time discretization for conservation laws*, SIAM J. Sci. Comput., 35 (2013), pp. A1137–A1160.
- [39] A. KURGANOV AND Y. LIU, *New adaptive artificial viscosity method for hyperbolic systems of conservation laws*, J. Comput. Phys., 231 (2012), pp. 8114–8132.
- [40] A. KURGANOV AND E. TADMOR, *New high-resolution central schemes for nonlinear conservation laws and convection-diffusion equations*, J. Comput. Phys., 160 (2000), pp. 241–282.
- [41] J. KUSCH AND M. FRANK, *Intrusive methods in uncertainty quantification and their connection to kinetic theory*, Int. J. Adv. Eng. Sci. Appl. Math., 10 (2018), pp. 54–69.
- [42] J. KUSCH, R. G. MCCLAREN, AND M. FRANK, *Filtered stochastic Galerkin methods for hyperbolic equations*, J. Comput. Phys., 403 (2020). Paper No. 109073.
- [43] K.-A. LIE AND S. NOELLE, *On the artificial compression method for second-order nonoscillatory central difference schemes for systems of conservation laws*, SIAM J. Sci. Comput., 24 (2003), pp. 1157–1174.
- [44] H. LIU, *A numerical study of the performance of alternative weighted ENO methods based on various numerical fluxes for conservation law*, Appl. Math. Comput., 296 (2017), pp. 182–197.
- [45] S. MISHRA, *Numerical methods for conservation laws with discontinuous coefficients*, in Handbook of numerical methods for hyperbolic problems, vol. 18 of Handb. Numer. Anal., Elsevier/North-Holland, Amsterdam, 2017, pp. 479–506.

- [46] S. MISHRA AND C. SCHWAB, *Monte-Carlo finite-volume methods in uncertainty quantification for hyperbolic conservation laws*, in Uncertainty quantification for hyperbolic and kinetic equations, vol. 14 of SEMA SIMAI Springer Ser., Springer, Cham, 2017, pp. 231–277.
- [47] S. MISHRA, C. SCHWAB, AND J. ŠUKYS, *Multi-level Monte Carlo finite volume methods for uncertainty quantification of acoustic wave propagation in random heterogeneous layered medium*, J. Comput. Phys., 312 (2016), pp. 192–217.
- [48] H. NESSYAHU AND E. TADMOR, *Nonoscillatory central differencing for hyperbolic conservation laws*, J. Comput. Phys., 87 (1990), pp. 408–463.
- [49] M. PETTERSSON, G. IACCARINO, AND J. NORDSTRÖM, *Polynomial chaos methods for hyperbolic partial differential equations*, Mathematical Engineering, Springer, Cham, 2015. Numerical techniques for fluid dynamics problems in the presence of uncertainties.
- [50] P. PETTERSSON, G. IACCARINO, AND J. NORDSTRÖM, *A stochastic Galerkin method for the Euler equations with Roe variable transformation*, J. Comput. Phys., 257 (2014), pp. 481–500.
- [51] G. POËTTE, B. DESPRÉS, AND D. LUCOR, *Uncertainty quantification for systems of conservation laws*, J. Comput. Phys., 228 (2009), pp. 2443–2467.
- [52] J. QIU AND C.-W. SHU, *On the construction, comparison, and local characteristic decomposition for high-order central WENO schemes*, J. Comput. Phys., 183 (2002), pp. 187–209.
- [53] V. V. RUSANOV, *The calculation of the interaction of non-stationary shock waves with barriers*, Ž. Vyčisl. Mat. i Mat. Fiz., 1 (1961), pp. 267–279.
- [54] L. SCHLACHTER AND F. SCHNEIDER, *A hyperbolicity-preserving stochastic Galerkin approximation for uncertain hyperbolic systems of equations*, J. Comput. Phys., 375 (2018), pp. 80–98.
- [55] A. SEN, *1D pressureless gas dynamics systems in a strip*. Submitted, preprint is available at <https://arxiv.org/pdf/2502.15927.pdf>.
- [56] C.-W. SHU, *Essentially non-oscillatory and weighted essentially non-oscillatory schemes*, Acta Numer., 5 (2020), pp. 701–762.
- [57] P. K. SWEBY, *High resolution schemes using flux limiters for hyperbolic conservation laws*, SIAM J. Numer. Anal., 21 (1984), pp. 995–1011.
- [58] E. TADMOR, *Convergence of spectral methods for nonlinear conservation laws*, SIAM J. Numer. Anal., 26 (1989), pp. 30–44.
- [59] J. TRYOEN, O. LE MAÎTRE, M. NDJINGA, AND A. ERN, *Intrusive Galerkin methods with upwinding for uncertain nonlinear hyperbolic systems*, J. Comput. Phys., 229 (2010), pp. 6485–6511.
- [60] N. WIENER, *The Homogeneous Chaos*, Amer. J. Math., 60 (1938), pp. 897–936.
- [61] D. XIU, *Numerical methods for stochastic computations*, Princeton University Press, Princeton, NJ, 2010. A spectral method approach.
- [62] D. XIU AND J. S. HESTHAVEN, *High-order collocation methods for differential equations with random inputs*, SIAM J. Sci. Comput., 27 (2005), pp. 1118–1139.